Article

Immunity

Virus-like Particles Identify an HIV V1V2 Apex-Binding Neutralizing Antibody that Lacks a Protruding Loop

Highlights

- VLPs and stabilized Env trimers identify HIV-1-neutralizing N90-VRC38 Ab lineage
- Co-crystal structure of Ab N90-VRC38.01 with scaffolded V1V2-Env apex
- N90-VRC38 lineage targets the apex of HIV-1 Env trimer with non-protruding loops
- New mechanism of Ab:trimer-apex binding informs V1V2 vaccine strategies

Authors

Evan M. Cale, Jason Gorman, Nathan A. Radakovich, ..., Peter D. Kwong, John R. Mascola, James M. Binley

Correspondence

pdkwong@nih.gov (P.D.K.), jmascola@nih.gov (J.R.M.), jbinley@sdbri.org (J.M.B.)

In Brief

To date, long recognition loops have been a hallmark of apex-targeting antibodies. Cale et al. identify a lineage of HIV-1-neutralizing antibodies that target the envelope trimer apex. The N90-VRC38 lineage uses a loop of average length—a feature that may make it a useful prototype for vaccine design.

Cale et al., 2017, Immunity *46*, 777–791
May 16, 2017
http://dx.doi.org/10.1016/j.immuni.2017.04.011

CellPress

Immunity
Article

Virus-like Particles Identify an HIV V1V2 Apex-Binding Neutralizing Antibody that Lacks a Protruding Loop

Evan M. Cale,[1,10] Jason Gorman,[1,10] Nathan A. Radakovich,[1] Ema T. Crooks,[2] Keiko Osawa,[2] Tommy Tong,[2] Jiaqi Li,[1] Raju Nagarajan,[3] Gabriel Ozorowski,[4] David R. Ambrozak,[1] Mangai Asokan,[1] Robert T. Bailer,[1] Anthony K. Bennici,[1] Xuejun Chen,[1] Nicole A. Doria-Rose,[1] Aliaksandr Druz,[1] Yu Feng,[5] M. Gordon Joyce,[1] Mark K. Louder,[1] Sijy O'Dell,[1] Courtney Oliver,[1] Marie Pancera,[1] Mark Connors,[6] Thomas J. Hope,[7] Thomas B. Kepler,[8] Richard T. Wyatt,[5] Andrew B. Ward,[4] Ivelin S. Georgiev,[3,9] Peter D. Kwong,[1,*] John R. Mascola,[1,*] and James M. Binley[2,11,*]
[1]Vaccine Research Center, National Institute of Allergy and Infectious Diseases, National Institutes of Health, Bethesda, MD 20892, USA
[2]San Diego Biomedical Research Institute, San Diego, CA 92121, USA
[3]Vanderbilt Vaccine Center, Vanderbilt University Medical Center, Nashville, TN 37232, USA
[4]Department of Integrative Structural and Computational Biology, The Scripps Research Institute, La Jolla, CA 92037, USA
[5]Department of Immunology and Microbial Science, The Scripps Research Institute, La Jolla, CA 92037, USA
[6]HIV-Specific Immunity Section, Laboratory of Immunoregulation, National Institute of Allergy and Infectious Diseases, National Institutes of Health, Bethesda, MD 20892, USA
[7]Department of Cell and Molecular Biology, Feinberg Medical School, Northwestern University, Chicago, IL 60611, USA
[8]Boston University Department of Microbiology, Boston, MA 02118, USA
[9]Department of Pathology, Microbiology, and Immunology, Vanderbilt University Medical Center, Nashville, TN 37232, USA
[10]These authors contributed equally
[11]Lead Contact
*Correspondence: pdkwong@nih.gov (P.D.K.), jmascola@nih.gov (J.R.M.), jbinley@sdbri.org (J.M.B.)
http://dx.doi.org/10.1016/j.immuni.2017.04.011

SUMMARY

Most HIV-1-specific neutralizing antibodies isolated to date exhibit unusual characteristics that complicate their elicitation. Neutralizing antibodies that target the V1V2 apex of the HIV-1 envelope (Env) trimer feature unusually long protruding loops, which enable them to penetrate the HIV-1 glycan shield. As antibodies with loops of requisite length are created through uncommon recombination events, an alternative mode of apex binding has been sought. Here, we isolated a lineage of Env apex-directed neutralizing antibodies, N90-VRC38.01-11, by using virus-like particles and conformationally stabilized Env trimers as B cell probes. A crystal structure of N90-VRC38.01 with a scaffolded V1V2 revealed a binding mode involving side-chain-to-side-chain interactions that reduced the distance the antibody loop must traverse the glycan shield, thereby facilitating V1V2 binding via a non-protruding loop. The N90-VRC38 lineage thus identifies a solution for V1V2-apex binding that provides a more conventional B cell pathway for vaccine design.

INTRODUCTION

Neutralizing antibodies (NAbs) are likely to be a key component of effective HIV-1 vaccine immunity (Mascola and Montefiori, 2010). NAbs interfere with HIV-1 infection by binding to envelope (Env) spikes (comprised of gp120/gp41 trimers) on virion surfaces, thereby blocking receptor engagement or membrane fusion (Overbaugh and Morris, 2012). The glycan shield encasing these trimers helps the virus to evade NAbs, in part because carbohydrates are self-antigens to which antibody (Ab) responses are likely regulated by tolerance. Nevertheless, most, if not all, HIV-1 broadly neutralizing antibodies (bnAbs) make some glycan contacts upon native Env trimer binding (Stewart-Jones et al., 2016).

HIV-1 vaccine candidates can induce autologous NAbs but largely fail to induce NAbs against other circulating (tier 2) strains (Crooks et al., 2015; de Taeye et al., 2015; McCoy and Weiss, 2013). In contrast, cross-reactive NAbs develop in ~50% of HIV-1 infections (Doria-Rose et al., 2010; Hraber et al., 2014). Isolating monoclonal NAbs from such donors affords opportunities to understand how they develop and may be useful as vaccine blueprints (Burton and Hangartner, 2016).

Monoclonal bnAbs fall into several epitope clusters that, together, cover most of the trimer surface (Pancera et al., 2014; Ward and Wilson, 2015). The consistent features in different bnAbs suggest that a limited number of repertoire solutions can effectively tackle this complex antigen (Kwong and Mascola, 2012; Mascola and Haynes, 2013). One group of bnAbs targets the gp120 V1V2 loop at the trimer apex and includes PG9/16, CH01-04, CAP256.VRC26.01-33, and PGT141-145/PGDM1400-1412 (Andrabi et al., 2015; Bonsignori et al., 2011; Doria-Rose et al., 2015; Doria-Rose et al., 2014; Gorman et al., 2016; McLellan et al., 2011; Moore et al., 2011; Pancera et al., 2010; Sok et al., 2014; Walker et al., 2009, 2011). These NAbs exhibit unusually long (> 24 amino acids [AA] by Kabat numbering) anionic third heavy chain complementarity determining regions (CDRH3) that are often tyrosine sulfated

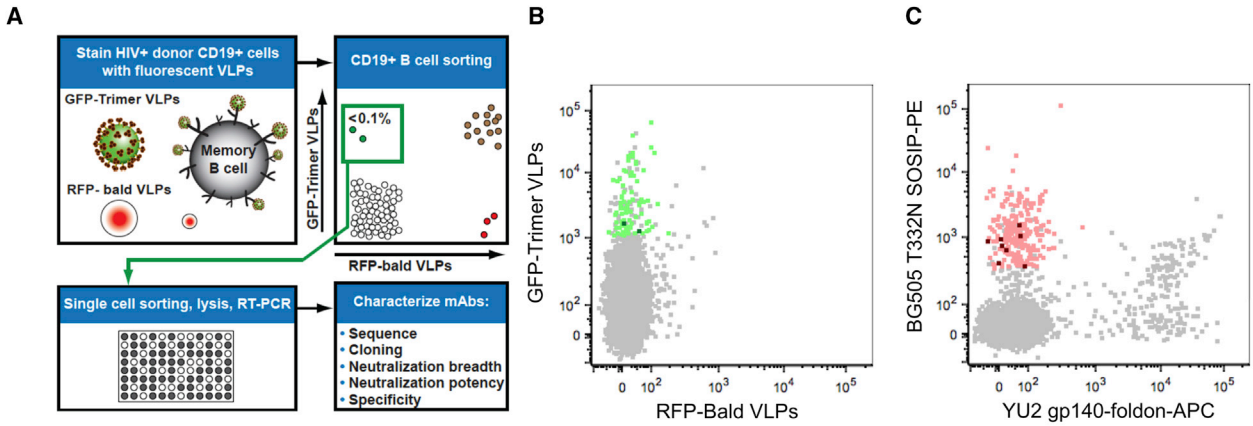

D

mAb	VH	JH	VH Mut. Freq. (%)*	CDRH3 length (AA)	CDRH3 Seq.	Vκ	Jκ	Vκ Mut. Freq. (%)*	CDRL3 length (AA)	CDRL3 Seq.
VRC38.01	3-13	6	17.5	16	GPESGWFYHYYWGLGV	2-28	4	8.5	10	MEARQTPRLT
VRC38.02			20.0		GPSSGWHLHYYFGMGL			10.9		MQSLETPRLS
VRC38.03	3-13	6	14.7	16	GPASGWWYHDYYGLYV	2-28	4	5.4	10	MQARQTPRLS
VRC38.04			18.9		GPSSGWHLHYYFGMGL			10.2		MQSLETPRLS
VRC38.05			18.6		GPSSGWHLHYYFGMGL			10.2		MQSLETPRLS
VRC38.06			17.5		GPESGWFYHYYFGLGV			11.2		MQARQTPRLS
VRC38.07			19.6		GPESGWFYHYYWGLGA			9.2		MEARQTPRLT
VRC38.08			15.4		GPTSGWWYHDYYGLDV			13.3		MQAVQTPRLS
VRC38.09			17.5		GPSSGWWYHYYFGLHL			5.4		MQARQTPRLS
VRC38.10			15.1		GPMSGWWYHDYYGLDV			11.9		MQAVETPRLS
VRC38.11			18.6		GPTSGWWYHDYYGLDA			15.3		MQAVQTPRLS

E

IC50 (μg/ml): >50 | 10-50 | 1-10 | 0.1-1 | <0.1

Env	Clade	VRC38.01	VRC38.02	VRC38.03	VRC38.04	VRC38.05	VRC38.06	VRC38.07	VRC38.08	VRC38.09	VRC38.10	VRC38.11
KER2018.11	A	0.018	0.018	0.211	0.024	0.076	0.037	0.029	0.088	0.140	0.082	0.078
Q23.17		0.006	0.025	0.188	0.021	>50	0.007	0.006	0.013	0.015	0.014	0.013
Q769.h5		>50	>50	>50	>50	>50	>50	>50	>50	>50	>50	>50
RW020.2		>50	>50	>50	>50	>50	>50	>50	>50	>50	>50	>50
BG505		0.025	>50	20.7	>50	>50	0.038	0.020	13.2	0.524	12.7	4.32
DJ263.8	AG	>50	>50	>50	>50	>50	>50	>50	>50	>50	>50	>50
TH966.8	AE	0.043	0.064	>50	0.056	>50	0.167	0.076	2.46	0.543	7.26	0.473
CNE59		>50	>50	>50	>50	>50	>50	>50	>50	>50	>50	>50
C1080.c3		0.008	>50	16.1	18.5	>50	0.007	0.010	1.95	0.081	7.47	0.323
6540.v4.c1	AC	>50	>50	>50	>50	>50	>50	>50	>50	>50	>50	>50
Q168.a2	AD	>50	>50	>50	>50	>50	>50	>50	>50	>50	>50	>50
6101.1	B	>50	>50	>50	>50	>50	>50	>50	>50	>50	>50	>50
BaL.01		5.86	>50	>50	>50	>50	0.807	13.1	1.21	>50	0.818	0.757
BG1168.01		12.3	3.99	>50	1.54	>50	>50	>50	>50	4.44	>50	>50
CAAN.A2		>50	>50	>50	>50	>50	>50	>50	>50	>50	>50	>50
JRCSF.JB		0.124	>50	0.204	>50	>50	0.052	0.072	1.13	0.234	12.9	0.253
JRFL.JB		0.686	>50	22.0	>50	>50	>50	>50	3.20	0.701	>50	>50
PVO.04		>50	>50	>50	>50	>50	>50	>50	>50	>50	>50	>50
THRO.18		>50	>50	>50	>50	>50	>50	>50	>50	>50	>50	>50
TRJO.58		>50	>50	>50	>50	>50	>50	>50	>50	>50	>50	>50
TRO.11		>50	>50	>50	>50	>50	>50	>50	>50	>50	>50	>50
YU2.DG		3.93	>50	>50	>50	>50	7.43	13.9	>50	>50	>50	>50
DU172.17	C	>50	>50	>50	>50	>50	>50	>50	>50	>50	>50	>50
DU156.12		0.565	>50	>50	>50	>50	1.40	0.441	6.24	14.7	5.74	4.52
DU422.01		22.4	>50	>50	>50	>50	>50	>50	>50	>50	>50	>50
ZA012.29		>50	>50	>50	>50	>50	>50	>50	>50	>50	>50	>50
ZM106.9		>50	>50	>50	>50	>50	>50	>50	>50	>50	>50	>50
CNE58		0.307	>50	>50	>50	>50	0.297	0.423	>50	>50	>50	>50
ZM55.28a		>50	>50	>50	>50	>50	>50	>50	>50	>50	>50	>50
57128.vrc15	D	>50	>50	>50	>50	>50	>50	>50	>50	>50	>50	>50
X1632.S2.B10	G	>50	>50	>50	>50	>50	>50	>50	>50	6.40	>50	>50
Mean IC_{50}		0.286	0.104	1.98	0.240	0.076	0.131	0.152	1.08	0.565	1.62	0.394
Breadth		42%	13%	19%	16%	3%	32%	35%	29%	32%	26%	26%

Figure 1. Trimer VLP Probes Identify a NAb Lineage of Moderate CDRH3 Length from an HIV-1-Infected Donor

(A) Overview of VLP-based NAb isolation. Negatively selected $CD19^+$ B cells were labeled with GFP-trimer VLPs and RFP-bald VLPs, then singly indexed sorted for GFP^+RFP^- B cells. Immunoglobulin genes were RT-PCR amplified. Desirable sequences were cloned, expressed, and characterized.

(legend continued on next page)

(excluding CH01-04) and project outward to penetrate the glycan shield and contact underlying protein. Abs with long CDRH3s naturally occur at low frequency due to a need for unusual recombination events and due to their regulation by tolerance (Briney et al., 2012a, 2012b; Haynes et al., 2012). Therefore, one goal of ongoing bnAb discovery is to identify NAbs with common repertoire features that are amenable to vaccine design.

NAb recovery efforts have taken two approaches: one involves high-throughput screening of memory B cell micro-cultures that identified known V1V2-directed bnAbs (Bonsignori et al., 2011; Doria-Rose et al., 2014; Walker et al., 2011; Walker et al., 2009); a second approach is to label desirable memory B cells with fluorescent "baits," followed by single-cell sorting and RT-PCR (Doria-Rose et al., 2015; Kong et al., 2016; Sok et al., 2014). Here, we used virus-like particles (VLPs) that present trimers in a natural membrane context (Crooks et al., 2011, 2015; Hicar et al., 2010) to probe memory B cells of a donor whose serum exhibited broad neutralization. We recovered a NAb lineage of moderate potency and breadth, N90-VRC38.01-11, that bound the V1V2 apex via an average length, non-protruding CDRH3, thereby revealing a new immunological solution to target the HIV-1 V1V2 apex site that may be more amenable for vaccine design.

RESULTS

VLPs Identify a New NAb Lineage with an Average-Length CDRH3

To develop VLPs as B cell probes, we co-transfected plasmids encoding SIV Gag, Env, Rev, and Gag-GFP (Figure S1). Concentrated supernatants were protease digested, resulting in "GFP-Trimer VLPs." SIV Gag and Gag-RFP plasmids were co-transfected to make "RFP-bald VLPs" as a counterstain. VLP labeling was verified using monoclonal Ab (mAb)-expressing Ramos cells and primary seronegative B cells (Figure S1). VLPs were then used to probe donor N90 B cells, whose serum neutralizes in a pattern that did not track with known bnAbs (Georgiev et al., 2013; Huang et al., 2014) (Figure S2A). Negatively selected N90 memory B cells were stained and gated for singlets, $CD3^-$, $CD8^-$, $CD14^-$, $CD19^+$, IgG^+, GFP^+, and RFP^- (Figure S1G). The extended positive shoulder imparted by trimer VLPs suggested specific labeling. We selected cells shown as green dots (Figure 1B). Despite a study in which VLPs recovered lipid-binding Abs (Hicar et al., 2010), RFP-bald VLP counterstaining was weak. The difference could relate to the higher VLP dose used for staining that allowed stringent washing (Figures S1C and S1D) but may also relate to the relatively dim RFP signal (Figure S1F). Following cell lysis, heavy- and light-chain variable segments were RT-PCR amplified, sequenced, and aligned. We prioritized clones with NAb features: (1) > 10% divergence from germline VH (heavy chain variable domain) nucleotide sequence; (2) long CDRH3 loops; (3) repeated recovery; or (4) insertion and deletion mutations. Two related clones, VRC38.01 and VRC38.02 (dark green dots in Figure 1B), were identified.

To recover additional VRC38 relatives, a second sort used PE-labeled BG505 SOSIP gp140 trimers (a near-native Env ectodomain mutant derived from the BG505 strain) as a positive probe. As VRC38.01 neutralizes the HIV-1 strain YU2 but does not bind to gp140F (a non-native, uncleaved Env ectodomain bearing a C-terminal foldon trimerization tag) derived from the same strain by ELISA (Figures S2D and S2E), APC-labeled YU2 gp140F trimers were used as a counterstain. PE^+APC^- sorting (Figure S1H) recovered nine more variants, VRC38.03–VRC38.11 (dark red dots in Figure 1C), all of which show little or no gp140F binding (Figures S2D and S2E).

VRC38 variants had a 16 AA CDRH3 and a 10 AA CDRL3, diverged 15%–20% nucleotides from germline VH3-13 (Figure 1D) and neutralized 3%–42% of a multi-clade 31-member virus panel (Figure 1E). Geometric mean IC_{50} titers (GMT) against sensitive viruses were 0.076–1.62 μg/mL. Although VRC38.09 was not as broad as VRC38.01, it neutralized one VRC38.01-resistant virus (X1632.S2.B10) (Figures 1E and S2A). We paired three VRC38 heavy-chain orphans from the second sort (Figure S2B) with the VRC38.01 light chain, one of which, VRC38.14, neutralized a VRC38.01-resistant strain (ZA012.29). Combining all lineage members, breadth against the 31-member virus panel was 48%. The broadest clone, VRC38.01, neutralized 30% of a panel of 208 Env-pseudoviruses (Table S1) and did not react with host antigens, as measured by cardiolipin ELISA (Figure S2F) and Hep2 (human epithelial type 2) staining (Figure S2G). Despite the donor's North American origin and clade B infection (Wu et al., 2012), VRC38 NAbs potently neutralized several clade A and AE viruses.

Neutralization profiles (Figure S2A) suggested that VRC38-like NAbs were not a dominant contributor to serum breadth. Several viruses were sensitive to the N90 serum, but not to VRC38 clones. Purified N90 serum immunoglobulin G (IgG) did not compete with VRC38.01 for binding to JR-FL native flexibly linked (NFL) trimers (Figure S2C), further suggesting low prevalence (< 1μg/mL; Figure S2C). Overall, the VRC38 lineage was infrequent in the donor plasma, exhibited 15%–20% germline divergence, modest neutralization potency and breadth, and no autoreactivity.

VRC38 Targets the V1V2-Trimer Apex

VRC38.01's ability to neutralize the YU2 strain (Figure 1E), despite poor YU2 gp140F binding (Figures S2D and S2E), suggested a quaternary epitope. By ELISA, VRC38.01 competed strongly with V1V2 bnAbs for binding trimer VLPs and, to a lesser extent, with glycan-V3 bnAb PGT121 (Figure 2A). Reciprocally,

(B) $GFP^+RFP^-IgG^+$ B cells (green dots) were selected. Dark green dots indicate VRC38.01 and VRC38.02.
(C) $PE^+APC^-IgG^+$ B cells (pink dots) were selected from SOSIP/gp140F stains. Dark red dots indicate VRC38.03–VRC38.11.
(D) VRC38 lineage heavy- and light-chain sequences were aligned to their closest V gene and J gene germline genes. Clones isolated using VLPs or SOSIP trimers were colored in green and red, respectively. *Mutation frequencies refer to percent nucleotide sequence divergence from germline V-gene sequences.
(E) VRC38.01–VRC38.11 neutralization of a multi-clade virus panel. GMTs of sensitive viruses (IC_{50} < 50μg/mL) and percent of viruses neutralized at IC_{50} < 50μg/mL (breadth) are shown. Although VRC38.05 neutralized only one virus, for comparison, this value was included in the "mean IC50" row. Neutralization assays are representative of two repeat assays.
See also Figures S1 and S2.

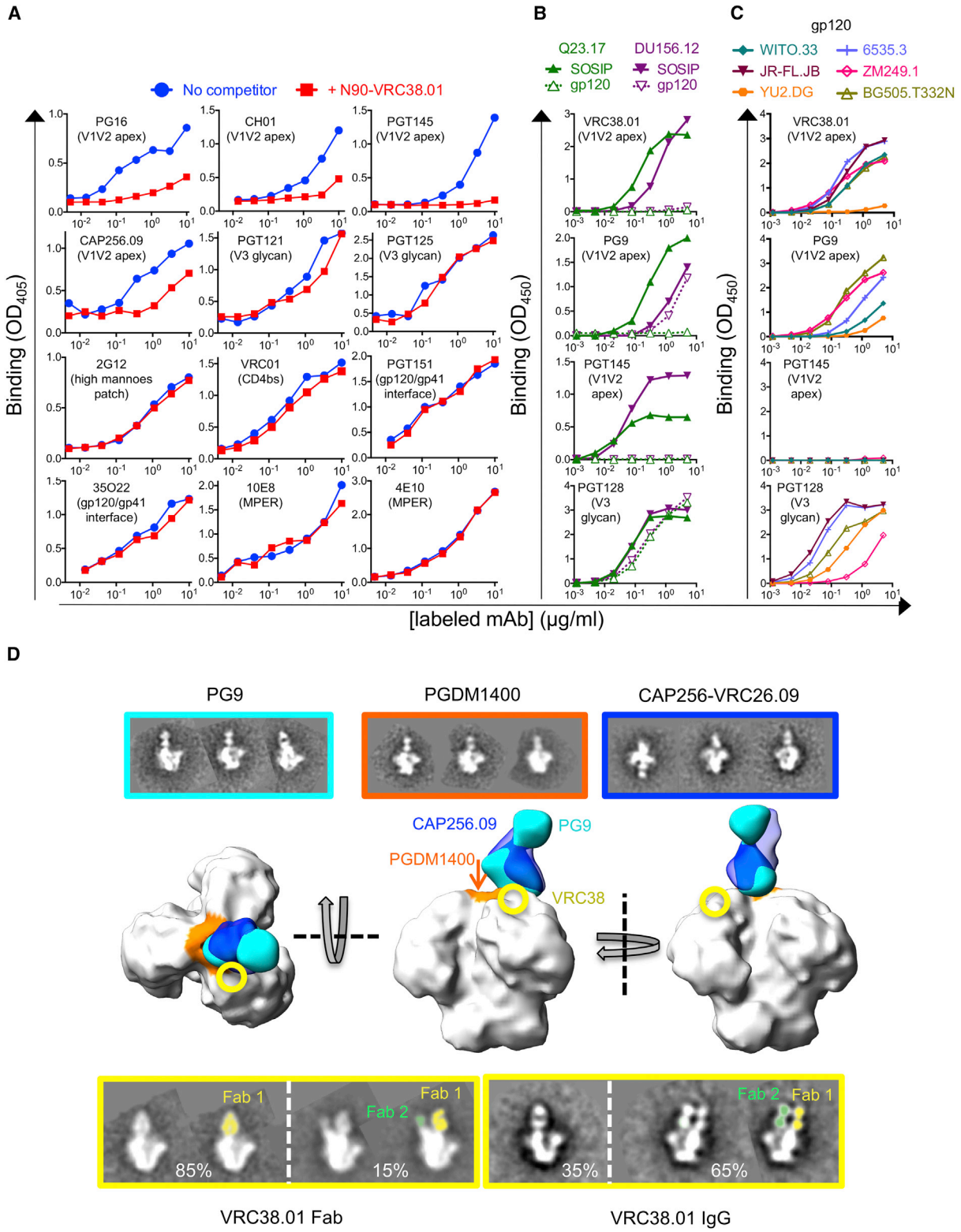

Figure 2. VRC38.01 Recognizes a Quaternary Epitope at the V1V2 Apex

(A) Excess VRC38.01 was used to compete with graded concentrations of biotinylated or strepII-tagged mAbs (VRC01 and 35O22) for binding to JR-FL SOS E168K or BG505 (for CAP256-VRC26.09) trimer VLPs by ELISA.

(legend continued on next page)

V1V2 bnAbs, PGT121 and, to a modest extent, glycan-V3 bnAb PGT125 inhibited VRC38.01 binding (Figure S3A). Neutralization of the JR-FL strain without a E168K mutation (Figure 1E) suggested a distinct V1V2 binding mode. Unlike for VRC38.01, this mutation was crucial for other V1V2 Nabs, and in some cases (e.g., with PG9, PG16, and CH01), an N189A mutation was also needed for full sensitivity (Figure S3B) (Doores and Burton, 2010).

To assess quaternary epitope dependency, we compared binding to monomeric gp120 and trimeric SOSIPs of sensitive strains, Q23.17 and DU156.12. Like PGT145, VRC38.01 bound to trimers, but not monomers, whereas glycan-V3 bnAb PGT128 bound to both forms of Env (Figure 2B). PG9 bound to DU156.12, but not Q23.17 gp120 (Figure 2B). Further analysis revealed VRC38.01 and PG9 bound to gp120 monomers from several neutralization-sensitive strains (Figure 2C). Together, these data suggest that these mAbs exhibit quaternary epitope preference, but that this is not a strict requirement for binding.

The footprint of VRC38.01 Fab (fragment, antigen-binding) was examined on BG505 SOSIP trimers by negative-stain electron microscopy (EM, Figure 2D). 2D class averages showed binding near the trimer apex. PG9 and CAP256-VRC26.09, for which 3D reconstructions were available (EMDB: 2241 and EMDB: 5856, respectively) appeared to straddle two gp120 protomers, binding adjacent to the 3-fold axis at a slightly off-vertical angle. 2D views of complexes with Fabs PDGM1400 or VRC38.01 were insufficient for 3D modeling. Nevertheless, class averages suggested footprints, as indicated in Figure 2D. VRC38.01's footprint was farther from the 3-fold axis and showed little interprotomer overlap. Overall, these data showed that VRC38.01 targets the V1V2 apex with a quaternary epitope preference.

VRC38.01 Binds "Off Center" and at Less than 3:1 Stoichiometry

V1V2 bnAbs typically bind the trimer with a stoichiometry of 1:1, in part because their footprints straddle gp120 protomers. 2D class averages of VRC38.01 Fab-trimer complexes by EM indicated one or two Fabs per trimer in ~85% or ~15% of cases, respectively (Figure 2D). Using VRC38.01 IgG, rather than the Fab, increased the proportion of complexes containing two Abs to 65% (Figure 2D), perhaps due to the increased avidity of two Fab arms; however, as the crystallizable fragment (Fc) of the IgGs was unresolved, it was unclear whether both Fabs originated from the same IgG in the EM images. Related to this point, VRC38.01 IgG was much more potent (17- to 170-fold) than its monovalent Fab, unlike PG9 (1- to 3.5-fold higher) and PGT145 (1- to 12-fold higher) (Figure S4A). Furthermore, real-time binding of VRC38.01 IgG to BG505 SOSIP trimers showed > 7-fold stronger binding over the Fab (Figure S4B), also supporting the idea that VRC38.01 IgG may engage trimers with both Fab arms simultaneously.

Binding stoichiometry was investigated by three further methods. First, we checked bnAb-mediated native trimer mobility shifts. 2G12 bound progressively to trimers with increasing concentrations, providing a reference ladder (Figure S4C). Saturating concentrations of all V1V2 NAbs bound at one copy per trimer (Figure S4C). In a second approach, we measured binding kinetics by biolayer interferometry (BLI). A standard curve was first generated with various trimer-NAb complexes of known ligand stoichiometries at saturation (Figure S4D). By interpolation, we inferred that ~2 copies of VRC38.01 (Fab or IgG) occupied the trimer (Figure S4D). In a third approach, we performed isothermal titration calorimetry (ITC) to assess VRC38.01 Fab binding to the BG505 native, flexibly linked (NFL) trimer, resulting in an estimate of N = 2.26 (Figure S4E). Previously, one copy PG9 Fab resulted in N = 0.6–0.8 (Julien et al., 2013; Sanders et al., 2013), 2 copies of PGT151 Fab resulted in N = 1.3 (Blattner et al., 2014) and 3 copies of PGT121 or 2G12 Fabs binding per trimer gave N = 2.3–2.4 (Sanders et al., 2013). Thus, an N value of 2.26 suggests that 2–3 VRC38.01 Fabs bind per trimer.

In addition to effects of avidity, the discrepancies above may relate to assay characteristics, with negative-stain EM and BN-PAGE emphasizing binding at equilibrium and BLI and ITC emphasizing on rate and maximum binding. Another contributing factor may be that the trimer strain and form differed between assays. Similar discrepancies were previously noted (Lee et al., 2015). Collectively, our data suggest that VRC38.01 recognition occurs at a sub-saturating antibody:trimer stoichiometry (Figures 2D and S4).

VRC38.01 Targets V1V2 Apex Glycans via a Non-protruding Loop

The off-center VRC38.01 footprint (Figure 2D), and its ability to neutralize viruses lacking a K168 residue (Figure S3B), suggested a unique binding mode. To obtain atomic-level detail, we co-crystallized Fab VRC38.01 with a V1V2-1FD6 scaffold (McLellan et al., 2011) derived from strain WITO.33. For reference, we first determined the unliganded VRC38.01 Fab structure to 1.6 Å, then we solved the complex structure to 3.5 Å by molecular replacement. Refinement yielded an R_{work}, R_{free} of 17.3, 20.2 and 21.3, 27.2 for the unliganded Fab and co-crystal structures, respectively (Figures 3A–3C, S5A, and Table S2). No significant binding-induced conformational changes were observed (Figures 3B, 3C, and S5A). Overall, these structures revealed V1V2 loop binding via protein-protein side-chain interactions with strands A, B, and C and extensive N156 and N160 glycan binding (Figures 3 and S5A).

(B) Binding to SOSIP.664 gp140 trimers and monomeric gp120 of strains Q23.17 and DU156.12 by ELISA.
(C) Binding to various monomeric gp120s by ELISA.
(D) Negative-stain EM of VRC38.01-SOSIP.664 complexes. Representative reference-free 2D class averages of known V1V2 bnAbs (top panel) and VRC38.01 IgG or Fab (bottom panel) complexed with BG505 SOSIP.664. In the middle panel, a ligand-free SOSIP model (low-pass filtered EM map created from X-ray coordinates of PDB: 4ZMJ) shows various V1V2 bnAb epitopes. PG9 and CAP256-VRC26.09 Fabs are shown by EM volumes and PGDM1400 and VRC38.01 footprints are indicated. For VRC38.01 Fab and IgG, proportions of complexes showing 1 Fab or 2 Fabs binding the trimer are shown. ELISA assays were repeated two times.
See also Figures S2, S3, and S4.

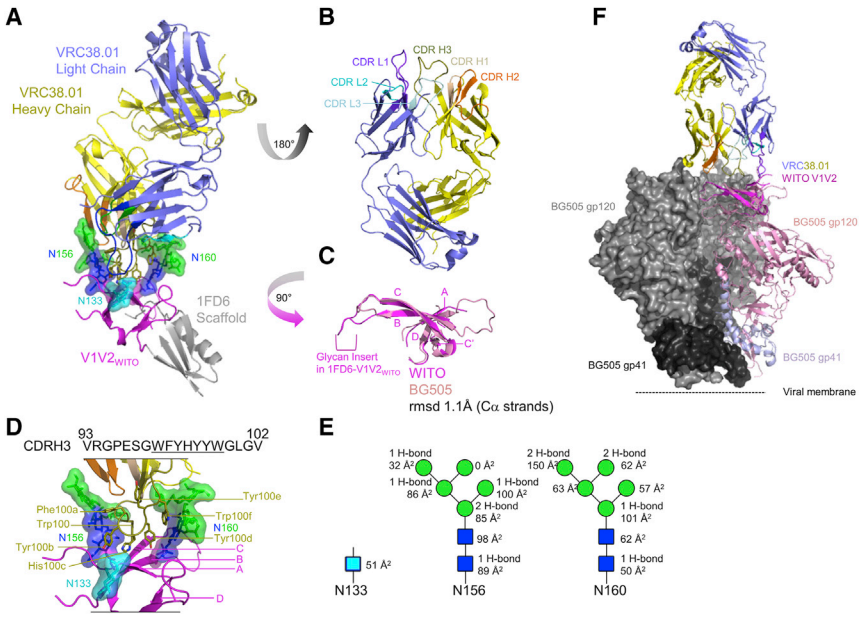

Figure 3. V1V2 Scaffold Complexes Reveal VRC38.01-Glycan Contacts and "Off-Center" Apex Binding

(A) A VRC38.01 V1V2-1FD6 scaffold co-crystal was solved at 3.5 Å. The heavy and light chains are shown in yellow and blue. The V1V2 (residues 126-196) and 1FD6 scaffold are shown in magenta and gray, respectively. Glycan mannoses are shown in green, and *N*-acetylglucosamine moieties are shown in blue.

(B) CDRs are highlighted for the bound Fab, which did not vary from the unbound Fab (RMSD 0.3 Å, not shown).

(C) The V1V2s of the WITO.33 scaffold (magenta) and BG505 SOSIP.664 trimer (pink, PDB: 4TVP) were aligned with an RMSD of 1.1 Å in the β sheets.

(D) The highly aromatic CDRH3 loop of VRC38.01 is enveloped by N156 and N160 glycans. Underlined CDRH3 AAs are shown in stick representation.

(E) A quantitative analysis of the mAb-glycan contacts is shown, with buried surface area of *N*-acetylglucosamine (blue squares) and mannose (green circles) residues indicated.

(F) Alignment of the VRC38.01-V1V2 complex with the BG505 SOSIP trimer structure (PDB: 4TVP) via the V1V2 domain.

See also Figure S5.

The V1V2 domain formed a 5-stranded β barrel as observed for near-native BG505 Env trimers (Pancera et al., 2014; Stewart-Jones et al., 2016), with a root-mean-square deviation (RMSD) of 1.1 Å across the β-strand residues (Figure 3C). Extensive VRC38.01-*N*-linked glycan contacts had buried surface areas of 490 Å^2 and 545 Å^2 for N156 and N160 glycans, respectively (Figures 3D and 3E). Mutations revealed that VRC38.01 was critically dependent on glycan N156 and heavily dependent on glycan N160 (Figure S5B). Minor contacts were observed between the light chain and glycan N133 (Figures 3A and 3E). Protein-protein contacts accounted for 470 Å^2 of buried surface area, including three hydrogen bonds and two salt bridges between V1V2 and the VRC38.01 heavy chain (Figure S5A).

Alignment of the complex to trimeric Env via the V1V2 (Figure 3F) confirmed the off-center footprint seen by EM (Figure 2D). Although direct VRC38.01 inter-protomer interactions were not observed, the Fab aligned closely to the N160 glycan of a neighboring gp120 protomer and the 9-residue disordered loop between positions N185 and S187 (Figure S5C). To probe these potential quaternary interactions, we engineered a glycan into the scaffold to mimic the neighboring N160 (scaffold insert position is shown in Figures 3C, 4I, and S5D). Although electron density observed for this engineered glycan was distal from the VRC38.01 epitope (Figure S5E), as N160 positioning is not precise, we were unable to rule out this interaction on the trimer. However, since VRC38.01 binds monomeric gp120 of several strains, N160 glycan binding to an adjacent protomer is probably not essential. The nine AAs following residue 185 in the V2 loop are disordered in available trimer structures and proximal to the framework 3 and CDRH1 of VRC38.01 (Figure S5C). However, mutagenesis suggested that this region did not affect VRC38.01, although other V2 bnAbs were marginally affected by some mutations within and proximal to this region (Figure S5F and Table S4). Analysis of the docked model in Figure 3F suggested that three VRC38.01 Fabs could potentially occupy one HIV-1 trimer with no clashes (overlap cutoff > 0.4 Å; Figure S5G). The sub-saturating VRC38.01 stoichiometry (Figures 2D and S4) may therefore stem from glycan or trimer structural heterogeneity (Liao et al., 2013). Based on the distance of the modeled Fab C-termini, VRC38.01 is unique in being potentially able to use both IgG arms to engage the trimer. The large differences in VRC38.01 IgG and Fab neutralization potency (Figure S4A) and trimer affinity (Figure S4B) lend indirect support to this idea. In summary, the cocrystal reveals N156 and N160 glycan-dependence but also light-chain contacts and a possibility to engage the trimer with both IgG arms.

VRC38.01 Makes Side-Chain-to-Side-Chain Contacts at the V2 Apex

VRC38.01 exhibits a near-charge-neutral 16 AA CDRH3, unlike other V1V2 NAbs that exhibit unusually long (> 24 AA) and anionic CDRH3s (Figure 4A) (Andrabi et al., 2015; Bonsignori et al., 2011; Doria-Rose et al., 2015; Gorman et al., 2016; McLellan et al., 2011; Walker et al., 2009, 2011). Although CH01 has greater breadth (53%) than its clonal variant CH03 (42%), we analyzed CH03 (AA sequence identity 83% in the VH and VL regions) due to the available V1V2-CH03 complex structure (Gorman et al., 2016). A comparison to normal Ab repertoire sequences (Shi et al., 2014) revealed the CDRH3 length of VRC38.01 to be within normal range but other V1V2 NAbs to be outliers (Figure 4B). VRC38.01 exhibits a near-neutral CDRH3 charge, which is common in the repertoire (Figure 4C). In contrast, other V1V2 NAb CDRH3 loops are negatively charged due to prevalent Glu and Asp residues and sulfated tyrosines (Figures 4A and 4E and 4F), which interact with the positively charged strand C (Andrabi et al., 2015; Bonsignori et al., 2011; Doria-Rose et al., 2015; Gorman et al., 2016; McLellan

A

bnAb	cohort	breadth	VH-gene	VH mutation (nucleotide)	CDRH3 length (AA)	CDRH3 sequence	Charge
VRC38.01	NIAID	30%	IGHV3-13	18%	16	CVRGPESGWFYHYYWGLGVW	-1
PG9	Protocol G	81%	IGHV3-33	14%	28	CVREAGGPDYRNGYNYYDFYDGYYNYHYMDVW	-6
CH03	CHAVI	42%	IGHV3-20	14%	24	CARGTDYTIDDQGIFYKGSGTFWYFDLW	-3
CAP256.25	CAPRISA	58%	IGHV3-30	12%	36	CAKDLREDECEEWWSDYYDFGKQLPCAKSRGGLVGIADNW	-7
PGT145	Protocol G	76%	IGHV1-8	17%	31	CLTGSKHRLRDYFLYNEYGPNYEEWGDYLATLDVW	-5

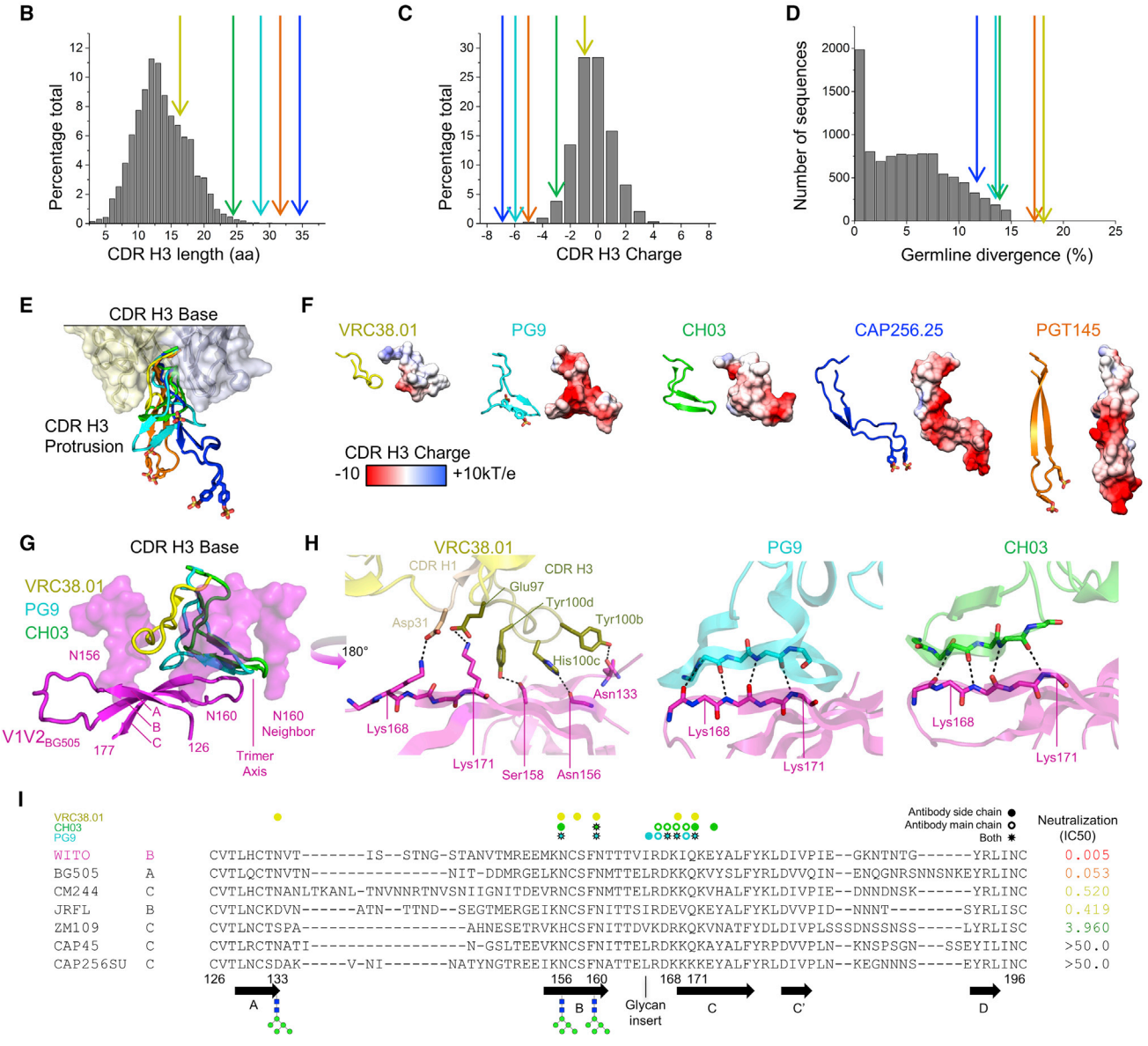

Figure 4. VRC38.01's Non-protuding HCDR3 Makes Side Chain-Side Chain Contacts at the V2 Apex

(A) Key features of prototype V1V2 mAbs, including their source, neutralization breadth (see Figure S6), germline VH gene use and divergence (nucleotide), CDRH3 length, sequence, and net charge. Negatively charged residues are shown in red, and sulfated tyrosines are underlined. Each NAb is color coded throughout.

(B) V1V2 mAb CDRH3 lengths (indicated by colored arrows) compared to the naive Ab repertoire distribution (Shi et al., 2014).

(C) Net V1V2 NAb CDRH3 charge compared to the naive Ab repertoire.

(D) V1V2 mAb germline divergence compared to the naive Ab repertoire.

(E) Alignment of the 5 mAb structures via their framework regions.

(F) Sulfated tyrosines are shown as sticks, and the electrostatic surface representation depicts charge.

(G) V1V2 mAb CDRH3 loops complexed with the V1V2 (magenta) and associated glycans (surface).

(legend continued on next page)

et al., 2011; Walker et al., 2009, 2011). Like other V1V2 NAbs, VRC38.01 substantially diverged from its germline (18%; Figures 4A and 4D).

Inspection of CDRH3-V1V2 contacts revealed VRC38.01 to bind a site more distal from the trimer axis than bound by PG9 and CH03 (Figure 4G), consistent with its footprint (Figure 2D). Like other V1V2 NAbs, VRC38.01 bound the N156 and N160 glycans of strand B (Figures 4G and S5B) but made protein-protein contacts solely through Ab side-chain interactions, in contrast to PG9 and CH03, which made extensive main-chain parallel strand-strand interactions with strand C residues 167–171, proximal to the inter-protomer interface (Figures 4H and S5A). The CDRH3 and CDRH1 loops of VRC38.01 hydrogen bonded to side chains of strands A, B, and C, including two salt bridges formed with residues K168 and K171 of strand C and heavy-chain residues D31 and E97, respectively (Figure 4H). This side-chain-dependent binding shortens the distance the CDRH3 loop must penetrate the glycan shield to reach underlying protein, enabling a short CDRH3 to suffice (Figures 4G–4I).

VRC38.01 Contacts Glycans N156 and N160 and Strand C but Clashes with Glycan N130

VRC38.01 neutralized 30% of a diverse panel of 208 pseudoviruses (Figure S6 and Table S1) at an IC_{50}<50 μg/mL, comparable to HJ16 and better than 2G12 (Figure S6A). VRC38's GMT against the 62 sensitive viruses (0.46 μg/mL) was lower than that of CH03 (0.54 μg/mL), 2G12 (1.56 μg/mL), b12 (1.00 μg/mL), 2F5 (1.63 μg/mL), and 8ANC195 (0.88 μg/mL) and was the same as HJ16 (0.46 μg/mL) (Figure S6A). VRC38.01 exhibited higher activity against 27 subtype A viruses (Table S1), where breadth and median IC_{50} were 52% and 0.043μg/mL, respectively (Table S1), though this increased activity was not seen on clade A recombinants (AG, AE, AC, AD) (Figure S6B). Overall, VRC38.01 exhibited modest potency and breadth.

Some bnAbs, including PG9 and PGT145, often plateau at < 100% neutralization, a phenomenon attributed in part to Env glycan heterogeneity (Doria-Rose et al., 2015; McCoy et al., 2015). To see if VRC38.01 exhibits this phenomenon, we determined its maximum % neutralization (Figure S6C) against all 208 virus strains in Table S1. To exclude weak neutralization, we only used data where IC_{50}s were < 1 μg/mL. Among this set of neutralized viruses, 80% and 72% were neutralized at > 90% and > 95%, respectively. Similar patterns were observed for PG9 and PGT145. Sub-saturating neutralization was somewhat more pronounced for CAP256-VRC26.25 and was highly prevalent for CH01, where only 5% of viruses were neutralized at a plateau > 95%. In summary, like other glycan V1V2 NAbs, VRC38.01 exhibits sub-saturating neutralization of some viruses.

An analysis of key V1V2 residues of our 208-member virus panel suggest that its side-chain-based binding mode (Figures 4H and 4I) may limit VRC38.01's breadth (Figure 5). Of the 146 VRC38.01-resistant strains, 135 related to variants at positions N130, N156, N160, K/R171, and Y173 (Figures 5A and 5B). Despite the VRC38.01 light-chain contact with the poorly conserved N133 glycan of the WITO.33 strain (Figures 3A and 3E), many N133-lacking viruses were VRC38.01 sensitive. Variation at positions N160, K/R169, and K/R171 explained all 39 PG9-resistant viruses (Figure S7). N156, N160, and K/R171 variants explained most CH03-resistant viruses, but 47 other resistant strains were unexplained (Figure S7). Critical residues became apparent when resistance mutations were mapped onto mAb complexes (Figure 5C). VRC38.01 sensitivity was enhanced by a K/R171 salt bridge with Glu97 of the heavy chain and by Y173-induced reorienting of glycan N156 (Figure 5C). Conversely, the N130 glycan appeared to cause a light-chain clash (Figure 5C). PG9 sensitivity was enhanced by glycan binding and by electrostatic interactions between Lys/Arg169 and Tys100 g, as well as Lys/Arg171 and Asp100i (Figure S7C). CH03 sensitivity was also enhanced via glycan interactions and by a salt bridge formed between Lys/Arg171 and Glu30 of the heavy chain (Figure S7D).

Introducing the N130 glycan into eight viruses that naturally lack this glycan reduced VRC38.01 sensitivity of all eight viruses (by > 50-fold in seven cases) (Figure 5D) but had less impact on PG9 recognition and even less on PGT145 recognition, which neutralized a N130 glycan-bearing DU422.01 mutant more effectively (Figure 5D). These findings are consistent with the latter bnAbs targeting epitopes closer to the trimer vertex. Reciprocal removal of the N130 glycan increased VRC38.01 sensitivity of BaL.26 and 25711-2.4 by > 40-fold and CAAN.A2 by > 7-fold (Figure 5E). VRC38.01 achieved 47.5% neutralization of strain DU172.17 at 50 μg/mL but did not neutralize the parent virus (Figure 5E). Again, the effect of removing glycan was less pronounced for PG9 and PGT145, and in fact reduced PG9 sensitivity of the 25711-2.4 strain (Figure 5E). Autologous N90 donor viral sequences (Wu et al., 2012) exhibited key contacts for VRC38 but had a sequon at N130 (Table S4) and were therefore VRC38.01-resistant. Upon N130D mutation, VRC38.01 reached 50% neutralization for three of viruses (Figure S7E). For the other five viruses tested, we detected increased VRC38.01 sensitivity that did not reach 50% at 100 μg/mL (Figure S7F).

Further mapping against strand A, B, and C mutants of the WITO.33 strain (Table S3) revealed sequon-disrupting S158A, N160K, and T162A mutations in strand B to reduce sensitivity to all four V1V2 NAbs (Table S3). Evaluation of the N156A mutant was complicated by its poor infection. Strand C mutations revealed K171 and Y173 to be critical for VRC38.01 but less so for other V1V2 NAbs. Analysis of BG505 and JR-CSF.JB strain mutants indicated similar VRC38.01 contacts (Table S3). However, unlike WITO.33, a Y173A mutation rendered these strains

(H) VRC38.01, PG9, and CH03 interactions with V1V2 strand C. VRC38.01 makes side-chain hydrogen bond contacts with K168 and K171 of strand C, N156 and S158 of strand B, and N133 of strand A. PG9 and CH03 make extensive main-chain parallel strand-strand interactions only with strand C. Side chain PG9 and CH03 contacts are shown in Figure S5A.

(I) Summary of V1V2 mAb contacts. Aligned V1V2 sequences are shown with their VRC38.01 sensitivities. VRC38.01, CH03, and PG9 contacts are shown as closed circles (side chain contacts), open circles (main chain contacts), and starred circles (both side chain and main chain contacts). Strands A–D, the N133, N156, and N160 glycans and the site of an engineered *N*-linked glycosylation insert between strands B and C (residues 165 and 166) placed at the approximate location of the N160 glycan of the neighboring protomer.

See also Figure S5.

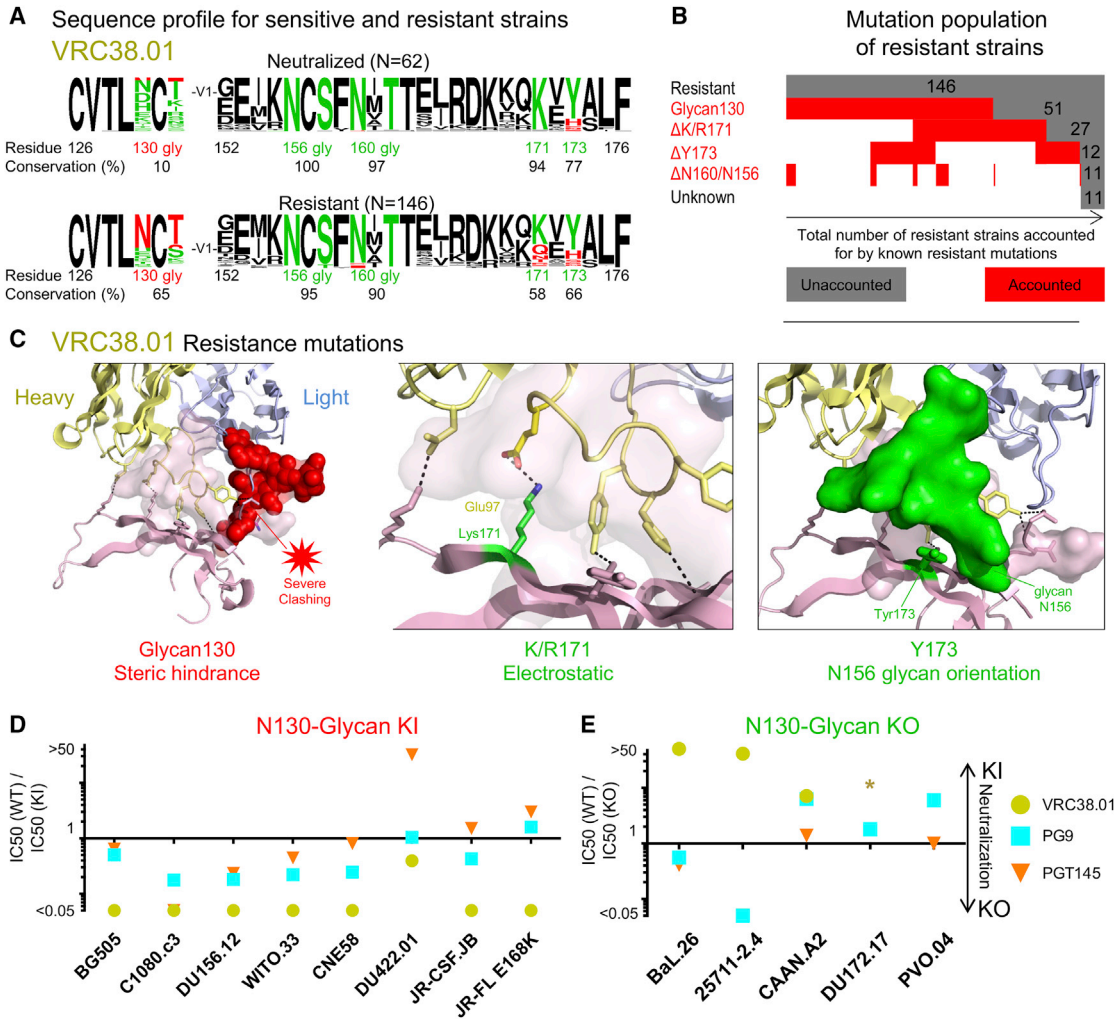

Figure 5. Breadth and Residue-Level Requirements of VRC38.01 Sensitivity

Prototype V1V2 mAbs were color coded as in Figure 4.

(A) Sequences of VRC38.01-sensitive (IC_{50} < 50 μg/mL) and -resistant (IC_{50} > 50 μg/mL) strains of our 208-member virus panel (Table S1) were rendered as logo plots, the height of each residue corresponding to its frequency. Residues and sequons (gly) linked with sensitivity (green) or resistance (red) with % conservation are shown.

(B) VRC38.01 resistance mutations in descending order of prevalence, with red bars indicating the number of viruses containing each resistance mutation. Vertical red bar overlaps indicate strains with multiple resistance mutations. Gray bars indicate the number of viruses with unaccounted resistance mechanisms.

(C) Structural analysis of VRC38.01 resistance mutations. A common glycan at residue 130 clashes with the VRC38.01 light chain (left). A favorable electrostatic interaction is formed between Glu97 of the heavy chain and a positive residue at position 171 on gp120 (center). Tyr173 appears to favorably orient the N156 glycan (right).

(D) Effects of N130 glycan knockin (KI) mutations on the V1V2 NAb sensitivity of viruses that naturally lack the N130 glycan. IC_{50} ratios against the parent and each KI virus are indicated. Ratios > 1 indicate increased sensitivity. Conversely, ratios of < 1 indicate reduced sensitivity.

(E) Effects of N130 glycan removal (KO) mutations on the V1V2 NAb sensitivity of viruses that naturally bear this glycan. IC_{50} ratios are shown as in (D). Asterisk (*) denotes maximum neutralization (50 μg/mL) of the DU172.17 mutant by VRC38.01 reached 47.8%, as compared to 0% for wild-type (WT). Neutralization assays were repeated two times.

See also Figures S6 and S7.

completely PGT145 resistant, and a K171A mutation rendered JR-CSF, but not BG505, resistant to CH01. Overall, the complete disruption of VRC38 recognition by mutations at K171 or Y173 confirmed the strand C dependency of this antibody. Together, sequence analysis of sensitive and resistant viruses (Figure 5) and mutation analysis (Table S3) indicated VRC38 resistance to be largely explained by a clash with glycan N130 or by a lack of key residues at positions 171 and 173 or by glycans at positions 156 and 160.

VRC38.01 Binding Tolerates Large Mannose Branches

The glycosylation inhibitor kifunensine prevents trimming of high mannose glycans, resulting in largely uniform $Man_9GlcNAc_2$ structures. Pseudoviruses prepared with this inhibitor are often

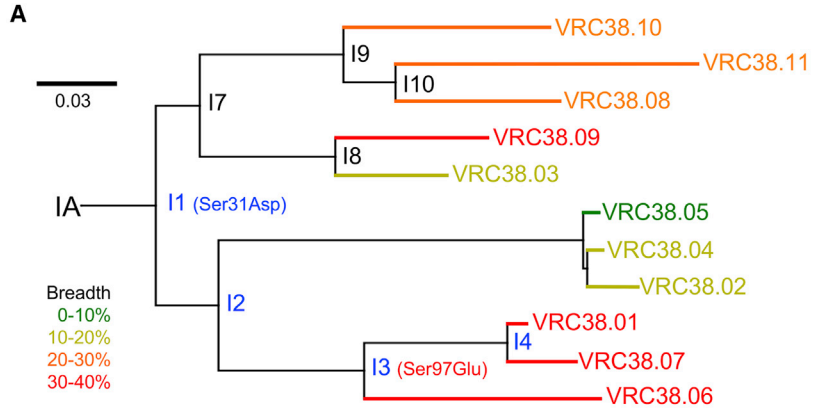

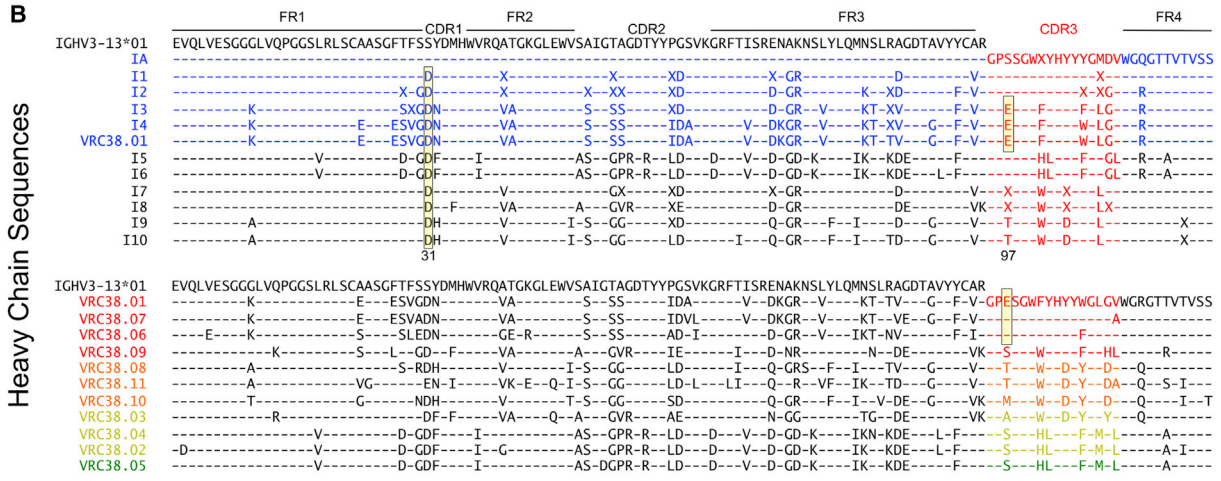

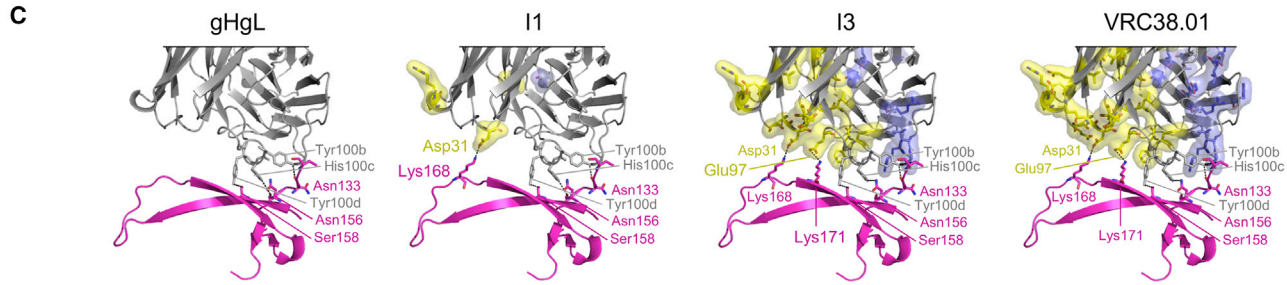

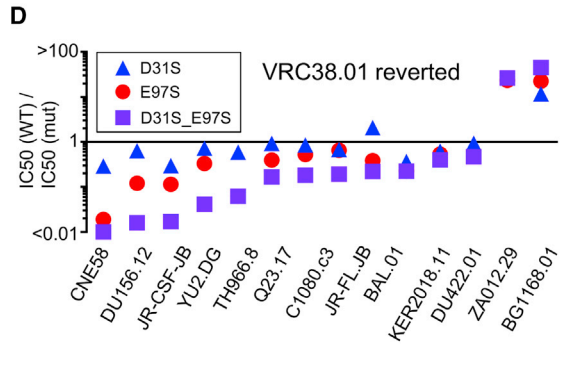

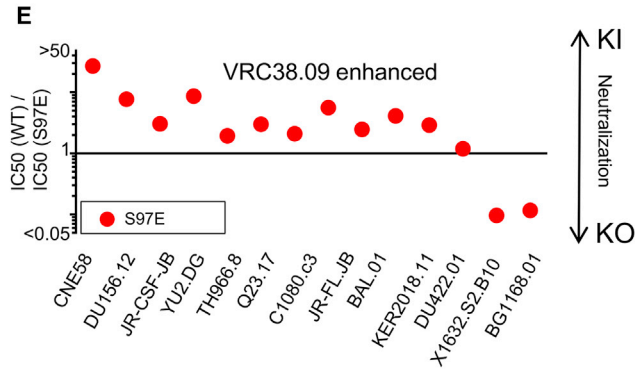

(legend on next page)

resistant to V1V2 bnAbs (Doores and Burton, 2010), perhaps due to changes in apex folding or because of a loss of mAb contacts with glycan sialic acid termini in the absence of this inhibitor (Amin et al., 2013; Pancera et al., 2013). We found that 83% (PG9), 92% (CH01), 94% (PGT145), and 69% (CAP256-VRC26.09) of kifunensine viruses were > 4-fold resistant (Table S5), but only 38% were resistant to VRC38.01. This further distinguishes VRC38.01 from other V1V2 mAbs and is in line with structural evidence suggesting that it can accommodate large mannose branches.

B Cell Ontogeny of VRC38 Neutralization

A phylogenetic tree of all 11 lineage members was generated, rooted by a common inferred ancestor (IA, Figure 6A). A variant with germline V-gene and J-gene reverted heavy (gH) and light (gL) chains that retained the mature CDRH3 was unable to neutralize (Table S1). However, hybrids consisting of mixed mature and reverted heavy- and light-chain partners, gHL and HgL, neutralized 19 and 18 strains of a 208-member panel, respectively (Table S1). Fourteen strains were sensitive to both hybrids, while others were neutralized by only one hybrid, indicating that both chains contribute to neutralization. When both the gHL and HgL Abs were effective, HgL potency was generally stronger, suggesting that the mature heavy chain plays a dominant role (Table S1). Overall, this suggests that VRC38 can neutralize ~9% of heterologous strains with no maturation of the V gene of one chain.

VRC38 heavy- and light-chain maturation was modeled as shown in Figure 6 and Table S6, respectively. S31D mutation likely occurred early in the VRC38 heavy chain (Figure 6A and boxed starting at sequence I1 in Figure 6B) and forms a salt bridge with a 97% conserved basic residue at position 168 (Figure 6C). However, data above (Figure 1E) suggests that, unlike other V1V2 NAbs, this contact is not essential (Figure S3B). Indeed, a D31S mutant modestly reduced neutralization of 11 of the 14 strains tested (Figure 6D). Three exceptions were BG1168.01 and JR-FL.JB, which were both more sensitive to the D31S mutant, and ZA012.29, which was insensitive to either the parent mAb or D31S mutant.

VRC38.01 shared a branch with broadly neutralizing lineage members VRC38.06 and VRC38.07, whose breadth may relate to a S97E mutation acquired at intermediate I3 (Figures 6A–6C), that forms a salt bridge with K171 of strand C (Figure 6C). E97S reversion reduced VRC38.01 neutralization to a larger degree than the D31S mutant. The two reversions together led to a substantial loss in neutralization, suggesting that both contacts contribute to VRC38.01 neutralizing activity (Figure 6D). VRC38.09, which is almost as broad as the three members of the VRC38.01 branch but almost 3-fold lower in potency, lacks the S97E mutation. However, a S97E mutant increased its potency against 12 of the 14 strains (Figure 6E). Exceptions were the uniquely VRC38.09-sensitive strain X1632.S2.B10 (Figure 1E) and the BG1168.01 strain. The behavior of the latter mirrored the effect of the reciprocal mutation on VRC38.01 (Figures 6D and 6E). Overall, VRC38.09's breadth developed independently from other clones, and the sensitivity of some strains to this variant depended on different somatic mutations.

VRC38-like NAbs May Be Prevalent in HIV-Infected Donors

To analyze VRC38-like bnAb prevalence, we used neutralization fingerprinting (Doria-Rose et al., 2017; Georgiev et al., 2013) to delineate bnAb specificities in a cohort of HIV-1-infected donors (Hraber et al., 2014). VRC38-like specificities (Figure 7A) were common, appearing in ~20% of plasmas, similar to the prevalence of PG9-like bnAbs. Analysis of the frequency of paired specificities (Figure 7B) revealed that VRC38-like and PG9-like signals were frequently paired with 10E8-like bnAbs—more frequently than 10E8-like pairings with other Abs. VRC38-like and PG9-like Abs also paired with each other, albeit at a much lower frequency than with 10E8. Overall, VRC38-like NAbs appear to be common in HIV-1 infection.

DISCUSSION

A growing number of recovered bnAbs now cover most of the Env-trimer surface. Many have unusual features that set a high bar for vaccine design and justify continued efforts to uncover new specificities. The VRC38 lineage provides a previously unknown solution for V1V2 apex binding, with potential advantages for vaccine elicitation. Abs with > 24 AA CDRH3s result from uncommon recombination events and, due to their typically autoreactive nature, may not survive B cell tolerance checkpoints (Briney et al., 2012a, 2012b). In contrast, the length and charge of the VRC38 CDRH3 is within the normal repertoire range. The lack of CDRH3 tyrosine sulfation or prevalent anionic side chains further advance VRC38 as a tangible vaccine blueprint, although this possibility will require formal testing.

Our fingerprint analysis suggested that VRC38-like Abs may be as prevalent as PGT128-like or PG9-like Abs. We are now

Figure 6. Structural Maturation of the VRC38 Lineage Sequence

(A) VRC38 phylogenetic tree branches were color-coded by their breadth against 31-member virus panel (Figure 1E). Computationally inferred intermediates are shown at nodes, with those leading to mature VRC38.01 shown in blue. S31D and S97E mutations are shown as they first appear.

(B) Heavy chain intermediate (upper set) and mature (lower set) sequences. In the upper set, intermediates leading to VRC38.01 are shown in blue. In the lower set, the 11 mature heavy chains are shown in descending order of breadth against the 31-member virus panel and are color-coded as in (A). D31 and E97 contacts are boxed.

(C) Structures of germline-reverted (gHgL, gray), I1 and I3 intermediates, and mature Ab complexed with WITO V1V2 (magenta). VRC38.01 heavy (yellow) and light (blue) chain V1V2 contacts are colored and shown in stick representation as they appear during maturation.

(D) Effects of reverting D31 and E97 residues to VRC38.01 inferred ancestor residues (S31 and S97) on mature VRC38.01 neutralization activity. Mutations, alone or in combination, were introduced into the VRC38.01 heavy chain and co-expressed with the mature VRC38.01 light chain, then assessed for neutralization activity. Ratios of IC_{50}s of WT VRC38.01 and mutant Abs are shown. Data are excluded for viruses in which both the WT and mutant Abs yielded IC_{50}s > 50μg/mL.

(E) Effects of mutating VRC38.09 S97 to E97. The heavy chain mutant was co-expressed with the mature VRC38.09 light chain and assessed for neutralization. Ratios of IC_{50}s of WT VRC38.09 and of the S97E mutant Ab are shown. Neutralization assays are representative of two repeat assays.

See also Table S6.

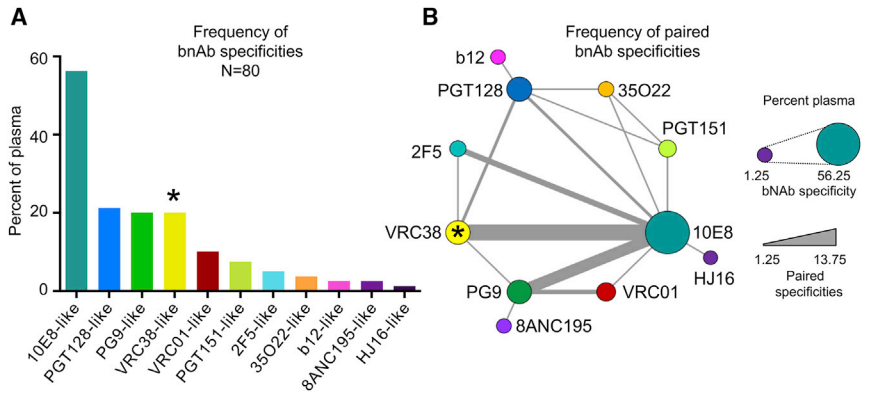

Figure 7. Fingerprint Analysis Suggests VRC38-like Specificities Are Common in HIV Infections

(A) Predicted frequency (percent of plasma) of different bnAb specificities. Bars were colored per Ab specificity, with bar height corresponding to frequency.

(B) Frequency of paired bnAb specificities in samples with predicted multiple specificities. Circle diameter corresponds to bnAb specificity frequencies. Edge widths correspond to the frequencies of specificity pairs.

mapping donor sera with VRC38-like signals and probing their B cells. Given its common features, VRC38-like NAbs might have been expected to be even more prevalent. However, an N130 glycan is found in > 60% of circulating viruses and is the single largest regulator of VRC38's breadth; N130 glycosylation may thus prevent VRC38-like bnAb development or facilitate escape. Accommodating glycan might therefore be a route to improved VRC38 breadth. We are now assessing additional donors and modifying our B-cell-probe strategy. For example, in a variation of the strategy in Figure 1C, B cells could be gated for positive binding to probes bearing a N130 glycan knock in mutation. It may also be useful to interrogate the N90 donor for VRC38 signatures by NGS and to probe samples from other donors that exhibit VRC38 fingerprint signatures. In a vaccine setting, N130 clash could be addressed using priming immunogens bearing an N130 "glycan hole" (Crooks et al., 2015) to promote VRC38-like NAb development and boosting with N130 glycan-containing immunogens to select for clones that can accommodate the glycan and thereby acquire greater breadth. Feasibility is supported by the observations that CD4bs-specific bnAb N6 evolved greater breadth by accommodating V5 loop glycans (Huang et al., 2016) and that the PGT121 family gained breadth by accommodating the N137 glycan (Garces et al., 2015).

Like other V1V2 NAbs (except PGT145 that derives from VH1-8), VRC38 derives from a VH3 family V gene, the most common VH family in human B cell repertoires. Moreover, like other V1V2 bnAbs, VRC38 VH diverged < 20% from its germline. This contrasts with the higher (~30%–40%) divergence of CD4bs bnAbs, making the V1V2 an attractive vaccine target. Indeed, the marginal protective efficacy observed in the RV144 Thai vaccine trial was related to V1V2-specific Abs, albeit Abs that were non-neutralizing and may therefore have exerted antiviral pressure by other mechanisms (Liao et al., 2013).

Some VRC38 binding requirements are akin to those of other V1V2 NAbs, including N156 and N160 glycan-dependent quaternary epitope preference and binding at less than 3:1 stoichiometry. In several other ways, however, VRC38 is unique. First, it binds farther away from 3-fold trimer axis, and both Fab arms of the VRC38.01 IgG may bind to a single trimer. It also exhibits a different binding mode that depends on CDRH1, CDRH3, and CDRL1 interactions with side chains of V1V2 strands A, B, and C, rather than main-chain interactions. This decreases the distance the CDRH3 must travel to penetrate the glycan shield. Since these contacts are conserved, VRC38 exhibits moderate breadth. Second, VRC38's CDRH3 exhibits a highly aromatic motif consisting of seven AAs (WFYHYYW), allowing it to accommodate glycans N156 and N160. Its unusual kifunensine resistance, along with structural data, suggest that it engages these glycans predominantly via their invariant stems. Thus, although glycan form variations may not affect VRC38, other V1V2 NAbs that depend, for example, on sialic acid contacts could be more prone to viral escape due to natural glycovariation (Amin et al., 2013; Pancera et al., 2013). Alternatively, the larger $Man_9GlcNAc_2$ structures promoted by kifunensine may distort packing at the trimer apex, perhaps having an impact on interprotomer binding by some V1V2 bnAbs (Julien et al., 2013), but not by VRC38 because it binds largely within one protomer. Unlike other V1V2 bnAbs (except CH01–CH04), VRC38.01's three CDRH3 tyrosines are not sulfated and lack anionic character. Specifically, "YYD"-binding motifs (with both tyrosines carrying charged sulfates) of PG9 and CAP256-VRC26 are absent. Thus, unlike other V1V2 bnAbs, VRC38.01 binding is not heavily dependent on electrostatic interactions.

Although VRC38.01 depends on residues K171 and Y173 of strand C, its partial K168 independence uniquely allows it to neutralize strains that are insensitive to other V2 mAbs. While K171 makes a clear electrostatic interaction with VRC38.01, Y173 may indirectly contribute by reorienting the N156 glycan. The lack of sensitivity of clade D viruses to VRC38.01 is explained by the fact that they typically lack the critical K/R171 and Y173 contacts. The higher clade A breadth of VRC38.01 was surprising, considering the donor's infection with a clade B virus and North American origin (Wu et al., 2012). However, clade A preference is also true for other V1V2 bnAbs, albeit those derived from African origin. However, although VRC38.01 breadth against clade A and clade A hybrid viruses was relatively high, it did not exceed that against the infecting clade B.

The cells from which the VRC38 lineage was cloned were sampled many years after infection, making it difficult to trace B cell ontogenies. A common unmutated ancestor and intermediates were nonetheless inferred from the 11 Ab sequences derived from the single time point. Neutralization by the V gene reverted VRC38.01 Ab and hybrid Abs with mature chains indicated both chains to contribute to neutralization, with the heavy chain making a greater contribution. Two affinity-matured residues on the heavy chain (S31D and S97E) that form salt bridges were present in the three broadest clones. The neutralizing

activity of the gHL variant suggests that while these interactions are not critical, they increase both breadth and potency.

One variant, VRC38.09, neutralized a virus that was insensitive to the VRC38.01 branch. Another virus was uniquely neutralized by the VRC38.14 variant heavy chain when paired with VRC38.01 light chain. Combining the number of viruses neutralized by all variants brought the VRC38 lineage breadth to 48%. It is unclear if a pathway could be found to neutralize these strains (and perhaps more) by a single VRC38 clone, especially since we only have access to one time point in this donor and thus can only approximate how the lineage might have evolved.

Our success in recovering VRC38 may in part be due to extensive VLP and B cell probe development. The broadest lineage member, VRC38.01, was identified using trimer VLPs as probes, and others were then isolated using SOSIP trimers. Thus, VLPs may complement existing B cell probes (Doria-Rose et al., 2015; Kong et al., 2016; Sok et al., 2014; van Gils et al., 2016). The high frequency of NAb clones in the VLP sort (2 out of 92; 2.2%) was consistent with specific staining. Nevertheless, certain suboptimal aspects of VLPs could be improved. Trimer VLPs imparted smeared staining in which VRC38.01 and VRC38.02 were relatively dim on the GFP axis, as opposed to a clearly separated positive population commonly seen with soluble SOSIP trimers. We are currently investigating alternative conjugation technologies (Mengistu et al., 2015) to tag VLPs with brighter fluorophores to enhance positive stain separation from background. Our observation that VRC38.01 contributes only partially to N90 serum breadth suggests that other bnAbs exist in this donor that we are now trying to recover.

In summary, a VLP probe recovered a VRC38 NAb lineage targeting the trimer apex without protruding binding loops by a previously unrecognized mechanism involving side-chain-to-side-chain interactions that reduced the distance an Ab loop must traverse the glycan shield. The genetic, functional, and structural analysis of this lineage, together with serological fingerprint analysis, suggest that similar NAbs may be relatively common during HIV-1 infection and may thus be amenable to vaccine elicitation.

STAR★METHODS

Detailed methods are provided in the online version of this paper and include the following:

- KEY RESOURCES TABLE
- CONTACT FOR REAGENT AND RESOURCE SHARING
- EXPERIMENTAL MODEL AND SUBJECT DETAILS
  - Human Subjects
  - Cell Lines
- METHOD DETAILS
  - Anti-HIV-1 Env Monoclonal Abs
  - Plasmids and Mutagenesis
  - Ramos-IgM Cell Line Production
  - VLP Production
  - Soluble Env Protein Production
  - HIV-1 Env-pseudotyped Virus Production
  - B Cell Sorting of Env Trimer-specific Clones
  - Single Cell RT-PCR of Ig Genes
  - mAb and Fab Production
  - Biotinylation of mAbs
  - ELISAs with Recombinant VLPs, gp120 and gp140
  - Measuring Probe Binding to mAb-Coated Beads
  - Neutralization Assays Using TZM-bl Cells
  - Neutralization Assays Using CF2 Cells
  - HEp-2 Cell Staining
  - Cardiolipin ELISA
  - Genetic Clustering and Phylogenetic Analysis
  - Blue Native PAGE-Western Blot
  - Negative-stain EM
  - Structural Analysis
  - Biolayer Interferometry
  - Surface Plasmon Resonance Analysis
  - Isothermal Titration Calorimetry
  - Neutralization Fingerprinting Analysis
- QUANTIFICATION AND STATISTICAL ANALYSIS
- DATA AND SOFTWARE AVAILABILITY

SUPPLEMENTAL INFORMATION

Supplemental information includes seven figures and six tables and can be found with this article online at http://dx.doi.org/10.1016/j.immuni.2017.04.011.

AUTHOR CONTRIBUTIONS

Conceptualization, E.M.C., J.G., N.A.R., P.D.K., J.R.M., and J.M.B.; Methodology, E.M.C., J.G., E.T.C., T.T., N.A.D.-R., T.B.K., A.B.W., I.S.G., J.R.M., and J.M.B.; Software, T.B.K. and I.S.G.; Validation, R.T.B. and M.K.L.; Investigation, E.M.C., J.G., N.A.R., E.T.C., K.O., T.T., J.L., R.N., G.O., D.R.A., M.A., A.K.B., Y.F., S.O., C.O., and T.B.K.; Resources, E.T.C., T.T., X.C., A.D., M.G.J., M.P., M.C., T.J.H., and R.T.W.; Writing – Original Draft, E.M.C., J.G., and J.M.B.; Writing – Review & Editing, E.M.C., J.G., P.D.K., J.R.M., and J.M.B.; Visualization, E.M.C., J.G., G.O., I.S.G., and J.M.B.; Supervision, A.B.W., I.S.G., P.D.K., J.R.M., and J.M.B.; Project Administration, E.M.C., J.G., P.D.K., J.R.M., and J.M.B.; Funding, P.D.K., J.R.M., and J.M.B.

ACKNOWLEDGMENTS

This work was supported by NIH grants RO1AI00790, RO1AI93278, and R33AI84714 (J.M.B.) U19AI117892-02 (T.B.K.), and by the intramural research program of the Vaccine Research Center, NIAID, NIH. We thank Bob Whalen (Altravax) for Rev and SIV Gag plasmids, Yang Dai (Scripps Research Institute) for the pAV MLV Gag plasmid, David Montefiori (Duke University) for large cohort serum-virus neutralization data, and Jonathan Stuckey for assistance with figures. Use of sector 22 (Southeast Region Collaborative Access team) at the Advanced Photon Source was supported by the US Department of Energy, Basic Energy Sciences, Office of Science, under contract #W-31-109-Eng-38. We thank donor N90 for participating. We thank J. Baalwa, D. Ellenberger, F. Gao, B. Hahn, K. Hong, J. Kim, F. McCutchan, D. Montefiori, L. Morris, J. Overbaugh, E. Sanders-Buell, G. Shaw, R. Swanstrom, M. Thomson, S. Tovanabutra, C. Williamson, and L. Zhang for contributing the HIV-1 Envelope plasmids used in our neutralization panel.

Received: October 14, 2016
Revised: February 9, 2017
Accepted: April 21, 2017
Published: May 16, 2017

REFERENCES

Amin, M.N., McLellan, J.S., Huang, W., Orwenyo, J., Burton, D.R., Koff, W.C., Kwong, P.D., and Wang, L.X. (2013). Synthetic glycopeptides reveal the glycan specificity of HIV-neutralizing antibodies. Nat. Chem. Biol. *9*, 521–526.

Andrabi, R., Voss, J.E., Liang, C.H., Briney, B., McCoy, L.E., Wu, C.Y., Wong, C.H., Poignard, P., and Burton, D.R. (2015). Identification of Common Features

in Prototype Broadly Neutralizing Antibodies to HIV Envelope V2 Apex to Facilitate Vaccine Design. Immunity *43*, 959–973.

Bhiman, J.N., Anthony, C., Doria-Rose, N.A., Karimanzira, O., Schramm, C.A., Khoza, T., Kitchin, D., Botha, G., Gorman, J., Garrett, N.J., et al. (2015). Viral variants that initiate and drive maturation of V1V2-directed HIV-1 broadly neutralizing antibodies. Nat. Med. *21*, 1332–1336.

Binley, J.M., Sanders, R.W., Clas, B., Schuelke, N., Master, A., Guo, Y., Kajumo, F., Anselma, D.J., Maddon, P.J., Olson, W.C., and Moore, J.P. (2000). A recombinant human immunodeficiency virus type 1 envelope glycoprotein complex stabilized by an intermolecular disulfide bond between the gp120 and gp41 subunits is an antigenic mimic of the trimeric virion-associated structure. J. Virol. *74*, 627–643.

Binley, J.M., Lybarger, E.A., Crooks, E.T., Seaman, M.S., Gray, E., Davis, K.L., Decker, J.M., Wycuff, D., Harris, L., Hawkins, N., et al. (2008). Profiling the specificity of neutralizing antibodies in a large panel of plasmas from patients chronically infected with human immunodeficiency virus type 1 subtypes B and C. J. Virol. *82*, 11651–11668.

Blattner, C., Lee, J.H., Sliepen, K., Derking, R., Falkowska, E., de la Peña, A.T., Cupo, A., Julien, J.P., van Gils, M., Lee, P.S., et al. (2014). Structural delineation of a quaternary, cleavage-dependent epitope at the gp41-gp120 interface on intact HIV-1 Env trimers. Immunity *40*, 669–680.

Bonsignori, M., Hwang, K.K., Chen, X., Tsao, C.Y., Morris, L., Gray, E., Marshall, D.J., Crump, J.A., Kapiga, S.H., Sam, N.E., et al. (2011). Analysis of a clonal lineage of HIV-1 envelope V2/V3 conformational epitope-specific broadly neutralizing antibodies and their inferred unmutated common ancestors. J. Virol. *85*, 9998–10009.

Briney, B.S., Willis, J.R., and Crowe, J.E., Jr. (2012a). Human peripheral blood antibodies with long HCDR3s are established primarily at original recombination using a limited subset of germline genes. PLoS ONE *7*, e36750.

Briney, B.S., Willis, J.R., Hicar, M.D., Thomas, J.W., 2nd, and Crowe, J.E., Jr. (2012b). Frequency and genetic characterization of V(DD)J recombinants in the human peripheral blood antibody repertoire. Immunology *137*, 56–64.

Burton, D.R., and Hangartner, L. (2016). Broadly Neutralizing Antibodies to HIV and Their Role in Vaccine Design. Annu. Rev. Immunol. *34*, 635–659.

Crooks, E.T., Tong, T., Osawa, K., and Binley, J.M. (2011). Enzyme digests eliminate nonfunctional Env from HIV-1 particle surfaces, leaving native Env trimers intact and viral infectivity unaffected. J. Virol. *85*, 5825–5839.

Crooks, E.T., Tong, T., Chakrabarti, B., Narayan, K., Georgiev, I.S., Menis, S., Huang, X., Kulp, D., Osawa, K., Muranaka, J., et al. (2015). Vaccine-Elicited Tier 2 HIV-1 Neutralizing Antibodies Bind to Quaternary Epitopes Involving Glycan-Deficient Patches Proximal to the CD4 Binding Site. PLoS Pathog. *11*, e1004932.

de Taeye, S.W., Ozorowski, G., Torrents de la Peña, A., Guttman, M., Julien, J.P., van den Kerkhof, T.L., Burger, J.A., Pritchard, L.K., Pugach, P., Yasmeen, A., et al. (2015). Immunogenicity of Stabilized HIV-1 Envelope Trimers with Reduced Exposure of Non-neutralizing Epitopes. Cell *163*, 1702–1715.

Doores, K.J., and Burton, D.R. (2010). Variable loop glycan dependency of the broad and potent HIV-1-neutralizing antibodies PG9 and PG16. J. Virol. *84*, 10510–10521.

Doria-Rose, N.A., Klein, R.M., Daniels, M.G., O'Dell, S., Nason, M., Lapedes, A., Bhattacharya, T., Migueles, S.A., Wyatt, R.T., Korber, B.T., et al. (2010). Breadth of human immunodeficiency virus-specific neutralizing activity in sera: clustering analysis and association with clinical variables. J. Virol. *84*, 1631–1636.

Doria-Rose, N.A., Schramm, C.A., Gorman, J., Moore, P.L., Bhiman, J.N., DeKosky, B.J., Ernandes, M.J., Georgiev, I.S., Kim, H.J., Pancera, M., et al.; NISC Comparative Sequencing Program (2014). Developmental pathway for potent V1V2-directed HIV-neutralizing antibodies. Nature *509*, 55–62.

Doria-Rose, N.A., Bhiman, J.N., Roark, R.S., Schramm, C.A., Gorman, J., Chuang, G.Y., Pancera, M., Cale, E.M., Ernandes, M.J., Louder, M.K., et al. (2015). New Member of the V1V2-Directed CAP256-VRC26 Lineage That Shows Increased Breadth and Exceptional Potency. J. Virol. *90*, 76–91.

Doria-Rose, N.A., Altae-Tran, H.R., Roark, R.S., Schmidt, S.D., Sutton, M.S., Louder, M.K., Chuang, G.Y., Bailer, R.T., Cortez, V., Kong, R., et al. (2017). Mapping Polyclonal HIV-1 Antibody Responses via Next-Generation Neutralization Fingerprinting. PLoS Pathog. *13*, e1006148.

Garces, F., Lee, J.H., de Val, N., de la Pena, A.T., Kong, L., Puchades, C., Hua, Y., Stanfield, R.L., Burton, D.R., Moore, J.P., et al. (2015). Affinity Maturation of a Potent Family of HIV Antibodies Is Primarily Focused on Accommodating or Avoiding Glycans. Immunity *43*, 1053–1063.

Georgiev, I.S., Doria-Rose, N.A., Zhou, T., Kwon, Y.D., Staupe, R.P., Moquin, S., Chuang, G.Y., Louder, M.K., Schmidt, S.D., Altae-Tran, H.R., et al. (2013). Delineating antibody recognition in polyclonal sera from patterns of HIV-1 isolate neutralization. Science *340*, 751–756.

Gomez, C.Y., and Hope, T.J. (2006). Mobility of human immunodeficiency virus type 1 Pr55Gag in living cells. J. Virol. *80*, 8796–8806.

Gorman, J., Soto, C., Yang, M.M., Davenport, T.M., Guttman, M., Bailer, R.T., Chambers, M., Chuang, G.Y., DeKosky, B.J., Doria-Rose, N.A., et al.; NISC Comparative Sequencing Program (2016). Structures of HIV-1 Env V1V2 with broadly neutralizing antibodies reveal commonalities that enable vaccine design. Nat. Struct. Mol. Biol. *23*, 81–90.

Haynes, B.F., Kelsoe, G., Harrison, S.C., and Kepler, T.B. (2012). B-cell-lineage immunogen design in vaccine development with HIV-1 as a case study. Nat. Biotechnol. *30*, 423–433.

Hicar, M.D., Chen, X., Briney, B., Hammonds, J., Wang, J.J., Kalams, S., Spearman, P.W., and Crowe, J.E., Jr. (2010). Pseudovirion particles bearing native HIV envelope trimers facilitate a novel method for generating human neutralizing monoclonal antibodies against HIV. J. Acquir. Immune Defic. Syndr. *54*, 223–235.

Hraber, P., Seaman, M.S., Bailer, R.T., Mascola, J.R., Montefiori, D.C., and Korber, B.T. (2014). Prevalence of broadly neutralizing antibody responses during chronic HIV-1 infection. AIDS *28*, 163–169.

Huang, J., Kang, B.H., Pancera, M., Lee, J.H., Tong, T., Feng, Y., Imamichi, H., Georgiev, I.S., Chuang, G.Y., Druz, A., et al. (2014). Broad and potent HIV-1 neutralization by a human antibody that binds the gp41-gp120 interface. Nature *515*, 138–142.

Huang, J., Kang, B.H., Ishida, E., Zhou, T., Griesman, T., Sheng, Z., Wu, F., Doria-Rose, N.A., Zhang, B., McKee, K., et al. (2016). Identification of a CD4-Binding-Site Antibody to HIV that Evolved Near-Pan Neutralization Breadth. Immunity *45*, 1108–1121.

Huson, D.H., Richter, D.C., Rausch, C., Dezulian, T., Franz, M., and Rupp, R. (2007). Dendroscope: An interactive viewer for large phylogenetic trees. BMC Bioinformatics *8*, 460.

Julien, J.P., Lee, J.H., Cupo, A., Murin, C.D., Derking, R., Hoffenberg, S., Caulfield, M.J., King, C.R., Marozsan, A.J., Klasse, P.J., et al. (2013). Asymmetric recognition of the HIV-1 trimer by broadly neutralizing antibody PG9. Proc. Natl. Acad. Sci. USA *110*, 4351–4356.

Kong, R., Xu, K., Zhou, T., Acharya, P., Lemmin, T., Liu, K., Ozorowski, G., Soto, C., Taft, J.D., Bailer, R.T., et al. (2016). Fusion peptide of HIV-1 as a site of vulnerability to neutralizing antibody. Science *352*, 828–833.

Kwon, Y.D., Pancera, M., Acharya, P., Georgiev, I.S., Crooks, E.T., Gorman, J., Joyce, M.G., Guttman, M., Ma, X., Narpala, S., et al. (2015). Crystal structure, conformational fixation and entry-related interactions of mature ligand-free HIV-1 Env. Nat. Struct. Mol. Biol. *22*, 522–531.

Kwong, P.D., and Mascola, J.R. (2012). Human antibodies that neutralize HIV-1: identification, structures, and B cell ontogenies. Immunity *37*, 412–425.

Lee, J.H., Leaman, D.P., Kim, A.S., Torrents de la Peña, A., Sliepen, K., Yasmeen, A., Derking, R., Ramos, A., de Taeye, S.W., Ozorowski, G., et al. (2015). Antibodies to a conformational epitope on gp41 neutralize HIV-1 by destabilizing the Env spike. Nat. Commun. *6*, 8167.

Li, M., Gao, F., Mascola, J.R., Stamatatos, L., Polonis, V.R., Koutsoukos, M., Voss, G., Goepfert, P., Gilbert, P., Greene, K.M., et al. (2005). Human immunodeficiency virus type 1 env clones from acute and early subtype B infections for standardized assessments of vaccine-elicited neutralizing antibodies. J. Virol. *79*, 10108–10125.

Liao, H.X., Bonsignori, M., Alam, S.M., McLellan, J.S., Tomaras, G.D., Moody, M.A., Kozink, D.M., Hwang, K.K., Chen, X., Tsao, C.Y., et al. (2013). Vaccine induction of antibodies against a structurally heterogeneous site of immune pressure within HIV-1 envelope protein variable regions 1 and 2. Immunity *38*, 176–186.

Mascola, J.R., and Haynes, B.F. (2013). HIV-1 neutralizing antibodies: understanding nature's pathways. Immunol. Rev. *254*, 225–244.

Mascola, J.R., and Montefiori, D.C. (2010). The role of antibodies in HIV vaccines. Annu. Rev. Immunol. *28*, 413–444.

McCoy, L.E., and Weiss, R.A. (2013). Neutralizing antibodies to HIV-1 induced by immunization. J. Exp. Med. *210*, 209–223.

McCoy, L.E., Falkowska, E., Doores, K.J., Le, K., Sok, D., van Gils, M.J., Euler, Z., Burger, J.A., Seaman, M.S., Sanders, R.W., et al. (2015). Incomplete Neutralization and Deviation from Sigmoidal Neutralization Curves for HIV Broadly Neutralizing Monoclonal Antibodies. PLoS Pathog. *11*, e1005110.

McLellan, J.S., Pancera, M., Carrico, C., Gorman, J., Julien, J.P., Khayat, R., Louder, R., Pejchal, R., Sastry, M., Dai, K., et al. (2011). Structure of HIV-1 gp120 V1/V2 domain with broadly neutralizing antibody PG9. Nature *480*, 336–343.

Mengistu, M., Ray, K., Lewis, G.K., and DeVico, A.L. (2015). Antigenic properties of the human immunodeficiency virus envelope glycoprotein gp120 on virions bound to target cells. PLoS Pathog. *11*, e1004772.

Migueles, S.A., Laborico, A.C., Shupert, W.L., Sabbaghian, M.S., Rabin, R., Hallahan, C.W., Van Baarle, D., Kostense, S., Miedema, F., McLaughlin, M., et al. (2002). HIV-specific CD8+ T cell proliferation is coupled to perforin expression and is maintained in nonprogressors. Nat. Immunol. *3*, 1061–1068.

Moore, P.L., Crooks, E.T., Porter, L., Zhu, P., Cayanan, C.S., Grise, H., Corcoran, P., Zwick, M.B., Franti, M., Morris, L., et al. (2006). Nature of nonfunctional envelope proteins on the surface of human immunodeficiency virus type 1. J. Virol. *80*, 2515–2528.

Moore, P.L., Gray, E.S., Sheward, D., Madiga, M., Ranchobe, N., Lai, Z., Honnen, W.J., Nonyane, M., Tumba, N., Hermanus, T., et al.; CAPRISA 002 Study (2011). Potent and broad neutralization of HIV-1 subtype C by plasma antibodies targeting a quaternary epitope including residues in the V2 loop. J. Virol. *85*, 3128–3141.

Ogura, T., Iwasaki, K., and Sato, C. (2003). Topology representing network enables highly accurate classification of protein images taken by cryo electron-microscope without masking. J. Struct. Biol. *143*, 185–200.

Overbaugh, J., and Morris, L. (2012). The Antibody Response against HIV-1. Cold Spring Harb. Perspect. Med. *2*, a007039.

Pancera, M., McLellan, J.S., Wu, X., Zhu, J., Changela, A., Schmidt, S.D., Yang, Y., Zhou, T., Phogat, S., Mascola, J.R., and Kwong, P.D. (2010). Crystal structure of PG16 and chimeric dissection with somatically related PG9: structure-function analysis of two quaternary-specific antibodies that effectively neutralize HIV-1. J. Virol. *84*, 8098–8110.

Pancera, M., Shahzad-Ul-Hussan, S., Doria-Rose, N.A., McLellan, J.S., Bailer, R.T., Dai, K., Loesgen, S., Louder, M.K., Staupe, R.P., Yang, Y., et al. (2013). Structural basis for diverse N-glycan recognition by HIV-1-neutralizing V1-V2-directed antibody PG16. Nat. Struct. Mol. Biol. *20*, 804–813.

Pancera, M., Zhou, T., Druz, A., Georgiev, I.S., Soto, C., Gorman, J., Huang, J., Acharya, P., Chuang, G.Y., Ofek, G., et al. (2014). Structure and immune recognition of trimeric pre-fusion HIV-1 Env. Nature *514*, 455–461.

Pettersen, E.F., Goddard, T.D., Huang, C.C., Couch, G.S., Greenblatt, D.M., Meng, E.C., and Ferrin, T.E. (2004). UCSF Chimera–a visualization system for exploratory research and analysis. J. Comput. Chem. *25*, 1605–1612.

Pugach, P., Ozorowski, G., Cupo, A., Ringe, R., Yasmeen, A., de Val, N., Derking, R., Kim, H.J., Korzun, J., Golabek, M., et al. (2015). A native-like SOSIP.664 trimer based on an HIV-1 subtype B env gene. J. Virol. *89*, 3380–3395.

Ross, S.A., Sarisky, C.A., Su, A., and Mayo, S.L. (2001). Designed protein G core variants fold to native-like structures: sequence selection by ORBIT tolerates variation in backbone specification. Protein Sci. *10*, 450–454.

Sanders, R.W., Derking, R., Cupo, A., Julien, J.P., Yasmeen, A., de Val, N., Kim, H.J., Blattner, C., de la Peña, A.T., Korzun, J., et al. (2013). A next-generation cleaved, soluble HIV-1 Env trimer, BG505 SOSIP.664 gp140, expresses multiple epitopes for broadly neutralizing but not non-neutralizing antibodies. PLoS Pathog. *9*, e1003618.

Sharma, S.K., de Val, N., Bale, S., Guenaga, J., Tran, K., Feng, Y., Dubrovskaya, V., Ward, A.B., and Wyatt, R.T. (2015). Cleavage-independent HIV-1 Env trimers engineered as soluble native spike mimetics for vaccine design. Cell Rep. *11*, 539–550.

Shi, B., Ma, L., He, X., Wang, X., Wang, P., Zhou, L., and Yao, X. (2014). Comparative analysis of human and mouse immunoglobulin variable heavy regions from IMGT/LIGM-DB with IMGT/HighV-QUEST. Theor. Biol. Med. Model. *11*, 30.

Sok, D., van Gils, M.J., Pauthner, M., Julien, J.P., Saye-Francisco, K.L., Hsueh, J., Briney, B., Lee, J.H., Le, K.M., Lee, P.S., et al. (2014). Recombinant HIV envelope trimer selects for quaternary-dependent antibodies targeting the trimer apex. Proc. Natl. Acad. Sci. USA *111*, 17624–17629.

Stewart-Jones, G.B.E., Soto, C., Lemmin, T., Chuang, G.-Y., Druz, A., Kong, R., Thomas, P.V., Wagh, K., Zhou, T., Behrens, A.-J., et al. (2016). Trimeric HIV-1-Env Structures Define Glycan Shields from Clades A, B, and G. Cell *165*, 813–826.

Tong, T., Crooks, E.T., Osawa, K., and Binley, J.M. (2012). HIV-1 virus-like particles bearing pure env trimers expose neutralizing epitopes but occlude non-neutralizing epitopes. J. Virol. *86*, 3574–3587.

van Gils, M.J., van den Kerkhof, T.L., Ozorowski, G., Cottrell, C.A., Sok, D., Pauthner, M., Pallesen, J., de Val, N., Yasmeen, A., de Taeye, S.W., et al. (2016). An HIV-1 antibody from an elite neutralizer implicates the fusion peptide as a site of vulnerability. Nat. Microbiol. *2*, 16199.

Walker, L.M., Phogat, S.K., Chan-Hui, P.Y., Wagner, D., Phung, P., Goss, J.L., Wrin, T., Simek, M.D., Fling, S., Mitcham, J.L., et al.; Protocol G Principal Investigators (2009). Broad and potent neutralizing antibodies from an African donor reveal a new HIV-1 vaccine target. Science *326*, 285–289.

Walker, L.M., Huber, M., Doores, K.J., Falkowska, E., Pejchal, R., Julien, J.P., Wang, S.K., Ramos, A., Chan-Hui, P.Y., Moyle, M., et al.; Protocol G Principal Investigators (2011). Broad neutralization coverage of HIV by multiple highly potent antibodies. Nature *477*, 466–470.

Ward, A.B., and Wilson, I.A. (2015). Insights into the trimeric HIV-1 envelope glycoprotein structure. Trends Biochem. Sci. *40*, 101–107.

Wu, X., Yang, Z.Y., Li, Y., Hogerkorp, C.M., Schief, W.R., Seaman, M.S., Zhou, T., Schmidt, S.D., Wu, L., Xu, L., et al. (2010). Rational design of envelope identifies broadly neutralizing human monoclonal antibodies to HIV-1. Science *329*, 856–861.

Wu, X., Wang, C., O'Dell, S., Li, Y., Keele, B.F., Yang, Z., Imamichi, H., Doria-Rose, N., Hoxie, J.A., Connors, M., et al. (2012). Selection pressure on HIV-1 envelope by broadly neutralizing antibodies to the conserved CD4-binding site. J. Virol. *86*, 5844–5856.

Yang, Z., Fang, J., Chittuluru, J., Asturias, F.J., and Penczek, P.A. (2012). Iterative stable alignment and clustering of 2D transmission electron microscope images. Structure *20*, 237–247.

Zalevsky, J., Chamberlain, A.K., Horton, H.M., Karki, S., Leung, I.W., Sproule, T.J., Lazar, G.A., Roopenian, D.C., and Desjarlais, J.R. (2010). Enhanced antibody half-life improves in vivo activity. Nat. Biotechnol. *28*, 157–159.

STAR★METHODS

KEY RESOURCES TABLE

REAGENT or RESOURCE	SOURCE	IDENTIFIER
Antibodies		
Monoclonal anti-HIV-1 Env 2G12	NIH AIDS Reagent Program; www.hiv.lanl.gov	Cat#1476
Monoclonal anti-HIV-1 Env b12	NIH AIDS Reagent Program; www.hiv.lanl.gov	Cat#2640
Monoclonal anti-HIV-1 Env VRC01	NIH AIDS Reagent Program; www.hiv.lanl.gov	Cat#12033; RRID: AB_2491019
Monoclonal anti-HIV-1 Env VRC07-G54W	John R. Mascola, NIH; www.hiv.lanl.gov	N/A
Monoclonal anti-HIV-1 Env VRC13	John R. Mascola, NIH; www.hiv.lanl.gov	N/A
Monoclonal anti-HIV-1 Env HJ16	NIH AIDS Reagent Program; www.hiv.lanl.gov	Cat#12138; RRID: AB_2491032
Monoclonal anti-HIV-1 Env PGT121	Dennis R. Burton, Scripps; www.hiv.lanl.gov	RRID: AB_2491041
Monoclonal anti-HIV-1 Env PGT125	Dennis R. Burton, Scripps; www.hiv.lanl.gov	RRID: AB_2491044
Monoclonal anti-HIV-1 Env PGT128	Dennis R. Burton, Scripps; www.hiv.lanl.gov	RRID: AB_2491047
Monoclonal anti-HIV-1 Env PG9	NIH AIDS Reagent Program; www.hiv.lanl.gov	Cat#12149; RRID: AB_2491030
Monoclonal anti-HIV-1 Env PG16	NIH AIDS Reagent Program; www.hiv.lanl.gov	Cat#12150; RRID: AB_2491031
Monoclonal anti-HIV-1 Env PGT145	Dennis R. Burton, Scripps; www.hiv.lanl.gov	RRID: AB_2491054
Monoclonal anti-HIV-1 Env PGDM1400	Dennis R. Burton, Scripps; www.hiv.lanl.gov	N/A
Monoclonal anti-HIV-1 Env CH01	NIH AIDS Reagent Program; www.hiv.lanl.gov	Cat#12561; RRID: AB_2491055
Monoclonal anti-HIV-1 Env CH03	NIH AIDS Reagent Program; www.hiv.lanl.gov	Cat#12563; RRID: AB_2491057
Monoclonal anti-HIV-1 Env CAP256.25 (VRC26.25)	John R. Mascola, NIH; www.hiv.lanl.gov	N/A
Monoclonal anti-HIV-1 Env CAP256.09 (VRC26.09)	John R. Mascola, NIH; www.hiv.lanl.gov	N/A
Monoclonal anti-HIV-1 Env PGT151	Dennis R. Burton, Scripps; www.hiv.lanl.gov	N/A
Monoclonal anti-HIV-1 Env 35O22	NIH AIDS Reagent Program; www.hiv.lanl.gov	Cat#12586
Monoclonal anti-HIV-1 Env 8ANC195	Michel C. Nussenzweig, Rockefeller University; www.hiv.lanl.gov	RRID: AB_2491037
Monoclonal anti-HIV-1 Env 10E8	NIH AIDS Reagent Program; www.hiv.lanl.gov	Cat#12294
Monoclonal anti-HIV-1 Env 2F5	NIH AIDS Reagent Program; www.hiv.lanl.gov	Cat#1475
Monoclonal anti-HIV-1 Env 4E10	NIH AIDS Reagent Program; www.hiv.lanl.gov	Cat#10091
Monoclonal anti-HIV-1 Env N90-VRC38.01-.14	John R. Mascola, NIH (This Paper)	N/A
Monoclonal anti-human CD3-APC-Cy7, clone SK7	BD Biosciences	Cat#557832
Monoclonal anti-human CD8-BV711, clone RPA-T8	Biolegend	Cat#301044
Monoclonal anti-human CD14-BV605, clone M5E2	Biolegend	Cat#301833
Monoclonal anti-human CD19-PE-Cy7, clone HIB19	BD Biosciences	Cat#560728
Monoclonal anti-human IgG-FITC, clone G18-145	BD Biosciences	Cat#555786
Monoclonal anti-human IgG-AlexaFluor 680, clone G18-145	Mario Roederer, NIH	N/A
HRP-conjugated anti-human IgG, Fcγ fragment Ab	Jackson ImmunoResearch	Cat#109-035-098
Purified mouse anti-human IgG Ab	BD Biosciences	Cat#555784
Human IgG (Fc), alkaline phosphatase (ALP)	Accurate Chemical and Scientific Corp.	Cat#JGH055008
Bacterial and Virus Strains		
208 HIV-1 Env-pseudotyped viruses	John R. Mascola, NIH (Kong et al., 2016)	N/A
Biological Samples		
PBMC from NIAID Donor N90	Mark Connors, NIH (Wu et al., 2012)	N/A
Serum from NIAID Donor N90	Mark Connors, NIH (Wu et al., 2012)	N/A
Serum from chronically infected donor 1686	James M. Binley, SDBRI (Binley et al., 2008)	N/A
Chemicals, Peptides, and Recombinant Proteins		
BG505.DS.T332N.SOSIP.664 gp140 trimer	Peter D. Kwong, NIH (This Paper)	N/A
YU2 gp140 foldon	John R. Mascola, NIH (This Paper)	N/A

(*Continued on next page*)

Continued

REAGENT or RESOURCE	SOURCE	IDENTIFIER
HIV-1 Env gp120 monomers	John R. Mascola, NIH (This Paper)	N/A
WITO V1V2 1FD6 scaffold	Peter D. Kwong, NIH (This Paper)	N/A
JR-FL.E168K-GFP virus-like particles (VLPs)	James M. Binley, SDBRI (This Paper)	N/A
Bald-RFP VLPs	James M. Binley, SDBRI (This Paper)	N/A
BG505 native, flexibly linked (NFL) trimer	Richard T. Wyatt (This Paper)	N/A
Kifunensine	Enzo Life Sciences	Cat#BML-S114-0001
LIVE/DEAD Fixable Violet Dead Cell Stain	Thermo Fisher	Cat#L34955
Streptavidin, R-phycoerythrin (SA-PE)	Thermo Fisher	Cat#S866
Streptavidin-allophycocyanin (SA-APC)	Thermo Fisher	Cat#S868
RNase OUT	Thermo Fisher	Cat#10777019
Random Hexamers	Gene Link	Cat#26-4000-03
10mM dNTP mix	Bioline	Cat#BIO-39053
EZ-Link Sulfo-NHS-Biotin	Thermo Fisher	Cat#21217
SigmaFAST p-nitrophenyl phosphate tablets	Sigma	Cat#N1891-5SET
SureBlue TMB Peroxidase Substrate	KPL	Cat#52-00-03
Streptavidin-alkaline phosphatase	Vector	Cat#SA-5100
Strep-Tactin alkaline phosphatase	IBA Life Sciences	Cat#2-1503-001
CompBead Anti-Mouse Ig, κ Compensation Particles	BD Biosciences	Cat#552843
DEAE-Dextran	Sigma	Cat#D9885-10G
Luciferase Cell Culture Lysis 5X Reagent	Promega	Cat#E1531
Protease Inhibitor Cocktail powder	Sigma	Cat#P2714
SigmaFast BCIP/NBT substrate	Sigma	Cat#B5655-5TAB
Nano-W Stain	Nanoprobes	Cat#2018
Protein A Plus Agarose	Pierce	Cat#22811
Critical Commercial Assays		
BirA Biotin-Protein Ligase Bulk Reaction Kit	Avidity	Cat#bulk BirA
Superscript III Reverse Transcriptase Kit	Thermo Fisher	Cat#18080093
HotStarTaq Plus DNA Polymerase Kit	QIAGEN	Cat#203603
Luciferase 1000 Assay System	Promega	Cat#E4550
ANA HEp-2 Test System – 25 Slides	Zeus Scientific	Cat#FA2400
Human B Cell Isolation Kit II	Miltenyi Biotec	Cat#130-091-151
QUANTA Lite ACA IgG III Assay	Inova Diagnostics	Cat#708625
4-12% Bis-Tris NuPAGE gel system	Thermo Fisher	Cat#NP0321BOX
Deposited Data		
N90-VRC38.01-VRC38.14 heavy chain nt sequences	This Paper	GenBank: KY_905214–905227
N90-VRC38.01-VRC38.11 light chain nt sequences	This Paper	GenBank: KY_905228–905238
N90-VRC38.01 Fab	This Paper	PDB: 5EWI
N90-VRC38.01 Fab bound to V1V2 scaffold	This Paper	PDB: 5VGJ
Experimental Models: Cell Lines		
Human: HEK293T	ATCC	Cat#CRL-3216, RRID: CVCL_0063
Human: HEK293S GnT1-	ATCC	Cat#CRL-3022, RRID: CVCL_A785
Human: HeLa-derived TZM-bl	NIH AIDS Reagent Program	Cat#8129-442, RRID: CVCL_B478
Canine: Canine thymus-derived CF2Th.CD4.CCR5	Joseph Sodroski (joseph_sodroski@dfci.harvard.edu), Dana-Farber Cancer Institute	N/A
Human: FreeStyle 293F	Thermo Fisher	Cat#R79007; RRID: CVCL_D603
Human: Expi293F	Thermo Fisher	Cat#A14527; RRID: CVCL_D615
Human: Burkitt's lymphoma-derived Ramos	JCRB Cell Bank	Cat# JCRB9119, RRID: CVCL_0597
Human: Ramos-VRC01	This Paper	N/A

(*Continued on next page*)

Continued

REAGENT or RESOURCE	SOURCE	IDENTIFIER
Ramos-PGT128	This Paper	N/A
Ramos-PGT145	This Paper	N/A
Oligonucleotides		
66 human immunoglobulin VH-, Vκ−, and Vλ-specific primers	John R. Mascola, NIH (Doria-Rose et al., 2015)	N/A
Recombinant DNA		
Plasmid pCAGGS	James M. Binley, SDBRI (This Paper)	N/A
Plasmid pNL4-3.Luc.R-E	James M. Binley, SDBRI (This Paper)	N/A
Plasmid pMV-2024	James M. Binley, SDBRI (This Paper)	N/A
Plasmid pMV-ERV	James M. Binley, SDBRI (This Paper)	N/A
Plasmid pMV-0932	James M. Binley, SDBRI (This Paper)	N/A
Plasmid pGag-GFP	James M. Binley, SDBRI (This Paper)	N/A
Plasmid pGag-RFP	James M. Binley, SDBRI (This Paper)	N/A
Software and Algorithms		
FlowJo v.9.9.4	FlowJo, LLC	https://www.www.flowjo.com; RRID: SCR_008520
IMGT/V-QUEST	International ImMunoGeneTics Information System; Marie-Paule Lefranc (marie-paule.lefranc@igh.cnrs.fr), University of Montpellier, France	www.imgt.org; RRID: SCR_012780
Cloanalyst	Thomas B. Kepler (tbkepler@bu.edu), Boston University	http://www.bu.edu/computationalimmunology/research/software/
HKL2000 Suite 6	HKL Research	www.hkl-xray.com
Phenix	Paul D. Adams (pdadams@lbl.gov), Lawrence Berkeley Laboratory	www.phenix-online.org; RRID: SCR_014224
Crystallographic Object-Oriented Toolkit (COOT) Software	Paul Emsley (paul.emsley@mrc-lmb.cam.ac.uk), Oxford University	https://www2.mrc-lmb.cam.ac.uk/personal/pemsley/coot/; RRID: SCR_014222
Molprobity	David C. Richardson (dcr@kinemage.biochem.duke.edu), Duke University	http://molprobity.biochem.duke.edu; RRID: SCR_014226
Microcal ORIGIN software	Microcal Software	http://en.freedownloadmanager.org/Windows-PC/Microcal-Origin.html; RRID: SCR_002815
Other		
carbon-coated Cu400 mesh grid	Electron Microscopy Sciences	Cat#EMS400-Cu
His1 Octet Biosensor Surface	ForteBio	Cat#18-5122
Biacore Sensor Chip CM5	GE Healthcare	Cat#BR100012

CONTACT FOR REAGENT AND RESOURCE SHARING

Further information and requests for resources and reagents should be directed to and will be fulfilled by the Lead Contact, James M. Binley (jbinley@SDBRI.org).

EXPERIMENTAL MODEL AND SUBJECT DETAILS

Human Subjects

Peripheral blood mononuclear cells (PBMCs) and sera were obtained from HIV-infected donor N90, who signed informed consent and participated in NIAID Institutional Review Board-approved protocols at the National Institutes of Health (NIH) (Doria-Rose et al., 2010; Georgiev et al., 2013; Migueles et al., 2002). At the time point studied, this donor was an antiretroviral therapy-naive slow progressor who had been diagnosed 23 years prior and exhibited broad serum neutralization, with viral load of 8,216 copies/ml, and 912 $CD4^+$ T cells/μl (Wu et al., 2012). A cohort of serum samples from donors infected with various HIV-1 clades assembled from various sources, including the Center for the AIDS Programme of Research in South Africa (CAPRISA), the Center

for HIV/AIDS Vaccine Immunology (CHAVI) and NIAID, as previously published (Hraber et al., 2014) was used for fingerprinting analysis. CAPRISA sample donors signed informed consent to participate in protocols approved by research ethics committees of the University of Kwazulu-Natal, the University of Cape Town, and the University of the Witwatersrand. CHAVI sample donors signed informed consent and participated in protocols approved by the Kilimanjaro Christian Medical Centre Research Ethics Committee, the Tanzania National Institutes for Medical Research Ethics Coordinating Committee, the Institutional Review Boards of the London School of Hygeine and Tropical Medicine and Duke University, and the NIH Institutional Review Board. Serum from chronically infected donor 1686, who signed informed consent to participate in protocol IRB-15-002-JB approved by the San Diego Biomedical Research Institute's Institutional Review Board, was previously shown to broadly neutralize via epitope(s) overlapping the CD4 binding site (Binley et al., 2008). PBMCs with no donor identifiers were also obtained from seronegative subjects for bait optimization; these donors participated in protocols approved by the NIH Institutional Review Board.

Cell Lines

Human embryonic kidney (HEK)-derived 293T, HEK293S N-acetylglucosaminyltransferase I-negative (GnTI-), and HeLa-derived TZM-bl cells were maintained in complete Dulbecco's Modified Eagle Medium (herein referred to as cDMEM) containing high-glucose Dulbecco's Modified Eagle Medium (DMEM, Thermo Fisher), 1X Penicillin-Streptomycin (Pen Strep, Thermo Fisher) and 10% fetal bovine serum (FBS, Gemini Bio Products) at 37°C/5% CO_2. Canine thymus-derived CF2Th.CD4.CCR5 cells were maintained in DMEM containing 1X Pen Strep, L-glutamine, 500 μg/ml G418, 150 μg/ml Hygromycin, and 10% FBS at 37°C/5% CO_2. FreeStyle 293F and Expi293F cells (both Thermo Fisher) were maintained in Freestyle 293 Expression Medium and Expi293 Expression Medium, respectively, at 37°C/10% CO_2 with shaking at 120 RPM. Human Burkitt's B cell lymphoma-derived Ramos cells were maintained in either DMEM containing 15% FBS and 1X Pen Strep or Roswell Park Memorial Institute 1640 medium (RPMI 1640, Thermo-Fisher) containing 10% FBS and 1X Pen Strep at 37°C/5% CO_2. In some cases, Ramos cells were engineered to stably express mature B cell receptors (BCR) IgM versions of VRC01, PGT145, and PGT128.

METHOD DETAILS

Anti-HIV-1 Env Monoclonal Abs

MAbs were obtained from the NIH AIDS Reagent Repository or from their originators. Further information can be found in the HIV Molecular Immunology Database (http://www.hiv.lanl.gov/) and in ref (Burton and Hangartner, 2016). MAbs included the following (originators given in parentheses): 2G12 (H. Katinger), directed to a glycan cluster on gp120; 39F and CO11 (J. Robinson), directed to the gp120 V3 loop; b12 (D. Burton), VRC01, VRC07-G54W, VRC13 (J. Mascola) and HJ16 (A. Lanzavecchia) directed to epitopes that overlap the CD4bs; PGT121, PGT125 and PGT128 (D. Burton) directed to epitopes involving the base of the V3 loop of gp120 and the N332 glycan; PG9, PG16, PGT145, PGDM1400 (D. Burton), CH01 and CH03 (B. Haynes) and CAP256.01-33 (J. Mascola), directed to quaternary, glycan-dependent V1V2 loop-directed epitopes; PGT151 (D. Burton), 35O22 (M. Connors), and 8ANC195 (M. Nussenzweig), directed to the gp120/gp41 interface; 10E8 (M. Connors), 2F5 and 4E10 (H. Katinger), directed to the gp41 membrane-proximal ectodomain region (MPER).

Plasmids and Mutagenesis

Plasmid pCAGGS was used to express JR-FL SOS E168K gp160ΔCT (Moore et al., 2006), featuring a 3 amino acid gp41 cytoplasmic tail, "SOS" mutations (A501C and T506C) to introduce a disulfide bond between gp120 and gp41 (Binley et al., 2000) and an E168K mutation to "knock in" V1V2 bnAb epitopes (Doores and Burton, 2010; Tong et al., 2012). Various Env expression plasmids were used to pseudotype viruses for neutralization assays and to express soluble gp140 glycoproteins, including uncleaved (UNC) YU2 gp140 foldon (gp140F) and BG505.DS.T332N.SOSIP.664 gp140 trimers (termed BG505 SOSIP trimers elsewhere for brevity) that feature the stabilizing 201C-433C disulfide (DS) mutation (Kwon et al., 2015). Some clones featured a C-terminal Avi tag (GLNDIFEAQKIEWHE) to enable biotinylation and fluororphore-streptavidin complexing (Doria-Rose et al., 2015). A codon optimized WITO strain V1V2 1FD6 scaffold was designed based on a previous construct (McLellan et al., 2011) and features an artificial N-terminal secretion signal (MRPTWAWWLFLVLLLALWAPARG), a C-terminal HRV3C cleavage site (GLEVLFQGP) followed by an 8-His tag and an engineered N-linked glycosylation site between strands B and C (residues 165 and 166) at the approximate location of the N160 glycan from the neighboring protomer. Env-deficient sub-genomic plasmids pNL4-3.Luc.R-E- and pSG3ΔEnv were described previously (Li et al., 2005). Plasmids pMV-2024 and pMV-ERV express full-length SIVmac251 (BK28) and MLV Gag, respectively. Plasmid pMV-0932 that expresses HIV-1 Rev was co-expressed whenever VLPs were produced using SIV or MLV Gag (Crooks et al., 2015). Plasmids pGag-GFP and pGag-RFP express full-length HIV-1 p55 Gag fused to eGFP and mCherry fluorophores, respectively, that for convenience are referred to as GFP and RFP throughout this study (Gomez and Hope, 2006). mAb heavy and light chain genes (in many cases codon optimized) were inserted into pVRC8400 to express IgG in Freestyle 293F or Expi293F cells, followed by protein A purification. In some cases, heavy chain plasmids were modified to add a C-terminal streptactin II tag (GGPGSAWSHPQFEKGGGSGGGSGGSAWSHPQFEK), a HRV3C recognition site (LEVLFQ/GP) inserted after K235 of the heavy chain and/or M428L/N434S mutations (indicated by a "-LS" suffix) (Zalevsky et al., 2010), to improve neonatal Fc receptor binding and in vivo half life.

Ramos-IgM Cell Line Production

Ramos cells were engineered to stably express mature B cell receptors (BCR) IgM versions of VRC01, PGT145, and PGT128.by lentiviral transduction of the cells using FEEKW-vectored light chain and IgM heavy chain-expressing lentiviruses. BCR-positive cells were identified by staining with both PE-conjugated mouse anti-human-kappa/lambda (BD Biosciences) and anti-human-IgM (Biolegend) by flow cytometry and sorted using a FACS Aria (BD Biosciences). Cells were amplified, assessed for BCR expression as before, and resorted for highest-staining cells if needed.

VLP Production

VLPs were produced by co-transfecting 293T or Freestyle 293F cells with plasmids expressing Env, Gag, and Rev (Crooks et al., 2015). Fluorescent VLPs were produced by also cotransfecting plasmids pGag-GFP or pGag-RFP. Two days later, supernatants were collected, filtered, precleared by centrifugation at 450Xg for 5 min, and concentrated either by tangential flow filtration or by centrifugation at 50,000Xg in a Sorvall SS34 rotor. "Trimer-VLPs" were made by digesting with 1 μL each of 1mg/ml proteinase K, subtilisin, and trypsin, and 1 μL of 2mg/ml chymotrypsin (Crooks et al., 2011; Tong et al., 2012). pNL4-3.Luc.R-E- based fluorescent VLPs were inactivated using 1mM aldrithiol (AT-2) before use as baits (Crooks et al., 2015). RFP-labeled "Bald-VLPs" were produced by co-expressing pMV-2024 (expressing SIV Gag) and pGag-RFP plasmids.

Soluble Env Protein Production

Trimeric Env constructs were expressed in various types of 293 cells and then purified by previously published methods (Bhiman et al., 2015; Doria-Rose et al., 2015; Stewart-Jones et al., 2016). For BG505.T332N.SOSIP proteins used for flow cytometric cell sorting, Avi-tagged proteins were biotinylated using the BirA Biotin-Protein Ligase Bulk Reaction Kit (Avidity, LLC) under the following conditions and reagents from the kit: 25 μL of 10X Biomix A, 25 μL of 10X Biomix B, 20 μg of BirA protein, and 180 μL of Avi-tagged SOSIP protein, incubated for 5 hr at 30°C with constant agitation. The mixture was buffer exchanged into SOSIP buffer containing 5mM HEPES, 150mM NaCl, and 0.02% NaN_3 in 30,000 MWCO Amicon Ultra-15 centrifugal filter units (EMD Millipore) over 5 rounds of spinning at 3000Xg, 4°C. Biotinylated SOSIP was then conjugated with streptavidin, R-phycoerythrin (SA-PE, Thermo Fisher) at a 1.17 SA-PE:SOSIP weight ratio (determined empirically). Briefly, biotinylated SOSIP was mixed with 1/5 the final volume of SA-PE and incubated for 20 min at 4°C with gentle rotation. Subsequent 1/5 increments of SA-PE were then added with 20 min incubations in between each addition. APC-conjugated YU2 gp140 foldon (gp140F) protein was biotinylated and conjugated to SA-allophycocyanin (SA-APC, Thermo Fisher) in the same manner at a 1.8 gp140F:SA-APC weight ratio (determined empirically).

V1V2 regions of various strains (residues 126-196, HXB2 numbering) were scaffolded onto a core variant of protein G (PDB: 1FD6) and were produced in HEK293S GnTI- cells and purified over Ni-NTA superflow resin (QIAGEN), then digested with HRV3C (Novagen) and purified over a 16/60 S200 size exclusion column (McLellan et al., 2011; Ross et al., 2001).

HIV-1 Env-pseudotyped Virus Production

Pseudoviruses for use in TZM-bl neutralization assays were produced in 293T cells by cotransfection of a pSG3ΔEnv backbone plasmid and a full HIV-1 Env gp160-encoding plasmid (Li et al., 2005). Briefly, $2X10^6$ cells in 20ml cDMEM were seeded in T75 flasks the day prior to cotransfection. For transfection, 40 μL of FuGene 6 reagent (Promega, Fitchburg, WI) was diluted into 800 μL of room-temperature Opti-MEM I reduced serum medium (Thermo Fisher), followed by addition of 10 μg of pSG3ΔEnv backbone plasmid. 3.3 μg of HIV Env plasmid was then added to the mixture, mixed, and incubated for 30 min at room temperature. Transfection mixture was then added to media of previously seeded 293T cells in the T75 flask and then distributed evenly on cells. The following day, media was replaced with 20ml fresh cDMEM. Virus was harvested the following day by filtering cell supernatants with 0.45 μm Steriflip units (EMD Millipore) and aliquotted.

Pseudoviruses for use in CF2 cell assays were produced in 293T cells by cotransfecting pNL4.3.Luc.R-E backbone plasmid and Env-expressing pCAGGS plasmid using polyethylenimine (PEI) Max (Polysciences). Briefly, $5X10^6$ cells were seeded on a 15cm tissue culture dish one day prior to transfection. On the day of transfection, 10 μg of pNL4.3.Luc.R-E and 10 μg of Env plasmid were mixed in 2ml of serum-free DMEM. 40 μL of 1mg/ml PEI Max (DNA:PEI ratio 1:2) was added and incubated at room temperature for 30 min. 11ml of cDMEM was then added to the transfection mixture. 293T cells were washed with PBS, and transfection mixture was added to the cells and distributed evenly. Following a 2 hr incubation at 37°C, culture dishes were washed with PBS, and 25ml of cDMEM was added to the cells for a 48 hr incubation at 37°C. Following incubation, virus was harvested by pelleting cell culture supernatant at 450Xg and filtering supernatant through a 0.8 μm filter.

For pseudoviruses containing point mutations, mutations were introduced into full HIV-1 Env-encoding plasmids using the QuickChange II Site-Directed Mutagenesis Kit (Agilent Technologies) according to the manufacturer's directions. For pseudoviruses produced under conditions containing kifunensine, 25 μM kifunensine was added at the time of plasmid cotransfection and replenished during the media change.

B Cell Sorting of Env Trimer-specific Clones

Frozen PBMCs ($\sim 5X10^7$ cells) were thawed in cDMEM containing 50 U/ml of benzonase (Novagen). For flow cytometric sorting, B cells were first enriched by negative magnetic bead selection using the Human B Cell Isolation Kit II (Miltenyi Biotec), then washed in PBS, resuspended in LIVE/DEAD Fixable Violet Dead Cell Stain (Thermo Fisher) and incubated for 30 min at 4°C. Cells were washed once in PBS and multicolor staining was performed using a panel of fluorophore-labeled mAbs directed to CD3

(APC-Cy7, clone SK7), CD8 (Brilliant Violet 711, clone RPA-T8), CD14 (Brilliant Violet 605, clone M5E2), CD19 (PE-Cy7, clone HIB19) and human IgG (fluorescein isothiocyanate [FITC] or Alexa Fluor 680, both clone G18-145). All mAbs were obtained from BD Biosciences except for those directed to CD8 and CD14 (Biolegend) and the anti-IgG-Alexa 680 Ab (custom-conjugated at the Vaccine Research Center, National Institutes of Health). Cells were also stained with fluorophore-tagged VLPs, BG505 SOSIP trimers or YU2 gp140F. All staining was performed at 4°C for 30 min, followed by two PBS/10% FBS washes and resuspension in PBS. Cells labeled as $CD3^-/CD8^-/CD14^-/CD19^+/IgG^+/GFP^+/RFP^-$ memory B cells were gated for VLP stains, or as $CD3^-/CD8^-/CD14^-/CD19^+/IgG^+$/BG505 SOSIP $trimer^+$/YU2 $gp140F^-$ for BG505 SOSIP trimer stains. Desirable cells were singly index-sorted on a FACS Aria sorter (BD Biosciences) into 96-well PCR plates (Denville Scientific) containing 20 μl/well lysis buffer consisting of 1U/μl RNase OUT (Thermo Fisher), 0.3125% Igepal CA-630, 1X SuperScript III First-Strand Buffer and 6.25 mM dithiothreitol (DTT) provided with the Superscript III Reverse Transcriptase kit (Thermo Fisher). Data were collected using FACSDiva software (BD Biosciences). Indexed sort data was analyzed using FlowJo software (FlowJo, LLC).

Single Cell RT-PCR of Ig Genes

RT-PCR amplification of IgG heavy and light chain genes was performed as described previously (Doria-Rose et al., 2015). 96-well plates containing single sorted cells were initially frozen at −80°C and thawed to maximize liberation of cellular mRNA. Total mRNA in each well of the 96-well plates was reverse transcribed using 200U/well Superscript III reverse transcriptase (Thermo Fisher), 2 μL of 10mM dNTP mix (Bioline) and 3 μL of 150 ng/μl random hexamers (Gene Link) under the following cycling parameters: 42°C 10 min, 25°C 10 min, 50°C 60 min, 94°C 5 min, and 4°C hold.

First strand cDNA was amplified in a 2-step multiplex nested PCR in which the first step used either mixed γ-, λ-, or κ-chain-specific primers (listed in (Doria-Rose et al., 2015). 50 μL κ- chain amplification reactions were performed using the QIAGEN HotStarTaq Plus DNA Polymerase Kit as follows (all reagents from HotStarTaq Plus kit unless otherwise noted): 1X QIAGEN PCR Buffer, 200 μM dNTP mix (Bioline), 500 μM $MgCl_2$, 1 μL of 50 μM 1^{st} round forward primer mix (5′L-Vk mix), 1 μL of 25 μM 1^{st} round reverse primer (3′Ck 543), 2U HotStarTaq Plus, and 5 μL of first-strand cDNA, under the following cycling parameters: 95°C 5 min; 50 cycles of 95°C 30 s, 58°C 30 s, 72°C 1min; 72°C 7 min; and 4°C hold. 40 μL γ- chain and λ-chain amplification reactions were performed similarly as follows: 1X QIAGEN PCR Buffer, 125 μM dNTP mix (Bioline), 1.4mM $MgCl_2$, 0.2 μL of 50 μM 1^{st} round forward primer mix (G1, G2, or G3 mix for γ- chain and 5′L-VL-RL mix for λ-chain), 0.2 μL of 25 μM 1^{st} round reverse primer (3′CgCH1 for γ- chain and 3′Cl for λ- chain), 2U HotStarTaq Plus, and 3 μL of first-strand cDNA. γ-chains were amplified under the following cycling parameters: 94°C 5 min; 50 cycles of 94°C 30 s, *x*°C 30 s, 72°C 55 s; 72°C 10 min; and 4°C hold, where *x* = 54°C for G1 mix, 48°C for G2 mix, and 52°C for G3 mix. λ-chains were amplified under the following cycling parameters: 95°C 5 min; 50 cycles of 95°C 30 s, 50°C 30 s, 72°C 1min; 72°C 7 min; and 4°C hold.

The second multiplex PCR step used mixed chain-specific primers that were complementary to regions slightly upstream and downstream of the first step forward and reverse primers, respectively. 50 μL γ-, κ- and λ- chain amplification reactions were performed using the QIAGEN HotStarTaq Plus DNA Polymerase Kit as follows (all reagents from HotStarTaq Plus kit unless otherwise noted): 1X CoralLoad PCR Buffer, 200 μM dNTP mix (Bioline), 1X Q Solution, 1 μL of 50 μM 2^{nd} round forward primer mix (5′L-VH mix + 5xwI-VH mix for γ- chain, 5′L-Vk-MS mix for κ- chain, and 5′L VI mix for λ- chain), 1 μL of 25 μM 2^{nd} round reverse primer (3′IgGint for γ- chain, 3′Ck 494 for κ- chain, and 3′XhoI Cl for λ- chain), 2U HotStarTaq Plus, and 3.5 μL 1^{st} round PCR product. γ-chains were amplified under the following cycling parameters: 95°C 5 min; 50 cycles of 95°C 30 s, 58°C 30 s, 72°C 1min; 72°C 7 min; and 4°C hold. κ-chains were amplified under the following cycling parameters: 95°C 5 min; 50 cycles of 95°C 30 s, 52°C 30 s, 72°C 1min; 72°C 7 min; and 4°C hold. λ-chains were amplified under the following cycling parameters: 95°C 5 min; 50 cycles of 95°C 30 s, 60°C 30 s, 72°C 1min; 72°C 7 min; and 4°C hold.

10 μL of each second round PCR product was loaded into 1% ethidium bromide-stained pre-cast gels (Embi Tec, San Diego, CA) and run at 120 V. Gels were visualized under ultraviolet light, and second round PCR products from wells where PCR-amplified bands were obtained were selected for sequencing by ACGT, Inc (Wheeling, IL). Alignments of sequences to germline V-, (D-), and J-genes and junctional analyses were performed using IMGT/V-QUEST (www.imgt.org). Clones of interest were identified by several criteria, including substantial germline mutations (> 10%) indicating a history of affinity selection, long CDRH3 loops and by repeated recovery in separate wells. Selected PCR products were cloned into pVRC8400 to construct heavy chain- and light chain-expressing plasmids for mAb expression and purification.

mAb and Fab Production

mAbs were expressed by cotransfection of Expi293F or Freestyle 293F cells (Thermo Fisher) with heavy chain- and light chain-expressing plasmids according to the cell manufacturer's directions. Following a 6-day incubation, transfection mixtures were pelleted by centrifugation and filtered through 0.22 μm Stericup filter units (EMD Millipore). Filtered supernatant was applied to a column containing a 1ml bed of Protein A Sepharose Fast Flow (GE Healthcare) equilibrated with Pierce Protein A IgG Binding Buffer (Thermo Fisher). The column was washed with Protein A IgG Binding Buffer, and mAb was eluted with Pierce IgG Elution Buffer (Thermo Scientific) and collected in a 1:10 volume of 1M Tris pH 8 solution. Antibodies were buffer-exchanged in PBS using 10,000 MWCO Amicon Ultra-15 centrifugal filter units (EMD Millipore) over three rounds of spinning.

For Fab production, the cleavage site (GLEVLFQGP) for the 3C protease of human rhinovirus (HRV3C) was inserted into the hinge region of the Ab heavy chain expression plasmid. Following expression and purification of mAb, the protein was subjected to HRV3C protease. Products were purified by gel filtration, and Fab fragments were collected for use in assays.

Biotinylation of mAbs

MAbs were biotinylated using EZ-Link Sulfo-NHS-Biotin (Thermo Fisher). Briefly, mAb was concentrated to 2-2.5 mg/ml (200-250 μL volume) and mixed with 15 μL of 50mg/ml Blue Dextran. mAb:Dextran mixture was applied to a Sephadex G25, NAP-5 column (GE Healthcare) previously washed 5X with 0.1M bicarbonate buffer (100mM $NaHCO_3$, pH 8.4). Antibody was eluted with 0.1M bicarbonate buffer, and the blue fraction containing mAb was collected. EZ Link Sulfo-NHS-Biotin (prepared as a 10mg/ml solution with dimethylsulfoxide) was added at 80 μg per 1mg mAb ratio and allowed to mix by rotating for 4 hr at room temperature. Biotinylated mAb was then loaded onto a Sephadex G25, PD-10 desalting column (GE Healthcare) previously washed 5X with a storage buffer containing 10mM Tris, 150mM NaCl, 0.1% NaN_3, pH 8.2. mAb was eluted with storage buffer, and the blue fraction containing biotinylated mAb was collected.

ELISAs with Recombinant VLPs, gp120 and gp140

Briefly, Immulon II plates were coated with either 20x concentrated VLPs (Tong et al., 2012), 5μg/ml recombinant gp120 monomer, or 5μg/ml gp140 trimers overnight at 4°C. Plates were washed with PBS twice and blocked. For VLP ELISA, blocking buffer was 4% BSA in 10% FBS/PBS, and for gp120 or gp140 ELISAs, blocking buffer was 4% milk in 0.05% Tween20/PBS. After 1h of blocking at room temperature and 2 washes with PBS or PBS containing 0.1% Tween 20 (PBS-T), serially diluted sera or mAbs were added in the following reaction buffers: 2% BSA in 10%FBS/PBS for VLP ELISA and 2% milk in PBS-T for gp120 or gp140 ELISAs. Plates were incubated for 1 hr at 37°C followed by 2 PBS or PBS-T washes. Species-specific alkaline phosphatase anti-Fc conjugates (Accurate) diluted in the corresponding reaction buffers at 1:5,000 were then added and plates were incubated at 37°C for 30 min. After a 4X wash with distilled H_2O, 50 μL of SigmaFAST p-nitrophenyl phosphate tablets (Sigma, St. Louis, MO) dissolved in distilled H_2O was added and incubated for 1 hr at room temperature in the dark. Reaction was stopped by adding 10 μL of 3N NaOH and detected at 405nm.

ELISAs using SOSIP gp140 trimers, gp140F, gp120 monomers, and V1V2 scaffolds were performed on Reacti-Bind 96-well polystyrene plates (Pierce). Briefly, plates were coated with 2 μg/ml of monomer/trimer in PBS overnight at 4°C. Following 6 washes with PBS-T and blocking for 1 hr at 37°C with B3T buffer (150 mM NaCl, 50 mM Tris-HCl, 1 mM EDTA, 3.3% FBS, 2% bovine serum albumin, 0.07% Tween 20, and 0.02% thimerosal), 5-fold serially diluted sera or mAbs were added in B3T buffer. After a 1 hr incubation at 37°C and 6 washes with PBS-T, plates were incubated with HRP-conjugated anti-human IgG, Fcγ fragment-specific antibody (Jackson ImmunoResearch, West Grove, PA) diluted 1:10,000 in B3T buffer for 1 hr at 37°C. After 6 washes with PBS-T, SureBlue TMB Substrate (KPL) was added, incubated for 10 min, and the reaction was stopped with 1N H_2SO_4 before measuring binding at 450nm.

Competitive VLP ELISAs was performed similarly to regular VLP ELISAs. Plates were coated, washed, and blocked in the same manner. After blocking, plates were washed twice with PBS, and 25 μL of competitor antibody was added at a fixed concentration. Following a 10 min incubation at 37°C, titrated biotinylated or Strep II-tagged mAbs were added and incubated for an additional hour at 37°C. After 2 washes with PBS, conjugates were added as follows: 1:300-diluted streptavidin-alkaline phosphatase (Vector) for biotinylated antibodies or 1:500-diluted streptactin-alkaline phosphatase (IBA Life Sciences) for Strep II-tagged antibodies. Plates were washed with distilled H_2O 4 times, 50 μL of SigmaFAST p-nitrophenyl phosphate tablets (Sigma) dissolved in distilled H_2O water was added, and plates were incubated for 1 hr at room temperature in the dark. Reaction was stopped by adding 10 μL of 3N NaOH before measuring binding at 405nm.

Measuring Probe Binding to mAb-Coated Beads

CompBead Anti-Mouse Ig, κ (BD Biosciences) were coated with mAbs for antigenic analysis of HIV-1 Env proteins and trimers. Briefly, 1ml of particles (beads) was pelleted at 1000Xg for 5 min, and supernatant was aspirated. Beads were resuspended in 1ml 0.5% bovine serum albumin (BSA) in PBS. 1 μg of Purified Mouse Anti-Human Ig κ Light Chain antibody (BD Biosciences) was added and allowed to incubate for 30 min at room temperature. 2ml of 0.5% BSA/PBS was added, beads were pelleted at 1000Xg for 5 min, and supernatant was aspirated. Beads were resuspended in 1ml of 0.5% BSA/PBS, and 1 μg of mAb was added, mixed, and incubated for 30 min at room temperature. 2ml of 0.5% BSA/PBS was added, beads were pelleted at 1000Xg for 5 min, and supernatants were aspirated. Beads were resuspended in 1ml 0.5% BSA/PBS for short-term storage of up to 1 week at 4°C. For staining, 50 μL of antibody-coated beads were mixed with different amounts of streptavidin-conjugated HIV-1 Env protein or trimer, incubated with 30 min at 4°C, and washed with 3ml of PBS. Beads were pelleted at 1000Xg for 5 min, supernatants were aspirated, and beads were resuspended in 300-500 μL PBS for flow cytometric analysis.

Neutralization Assays Using TZM-bl Cells

10 μL of 5-fold serially diluted mAbs or patient serum in cDMEM was incubated with 40ul of diluted HIV-1 Env-pseudotyped virus and incubated for 30 min at 37°C in a 96-well tissue culture plate. 20 μL of TZM-bl cells (10,000 cells/well) with or without 70 μg/ml DEAE-Dextran was then added and incubated overnight at 37°C. Each experiment plate also had a column of cells only (no Ab or virus) and a column of virus only (no Ab) as controls for background TZM-bl luciferase activity and maximal viral entry, respectively. The following day, all wells received 130 μL of fresh cDMEM and were incubated overnight at 37°C. The following day, media was aspirated from wells, and 50 μL of 1X Cell Culture Lysis Reagent (Promega) in distilled H_2O was added to cells. Lysates were shaken at 600RPM for 15 min, and 30 μL of lysate was transferred to OptiPlate black plates (Perkin Elmer). Luminometry was performed on a Perkin Elmer Model #1420-061 luminometer using the Promega Luciferase Assay System reagent (reconstituted in buffer provided with the kit,

equilibrated to room temperature). Percent neutralization is determined by calculating the difference in average RLU between virus only wells (cells + virus column) and test wells (cells + serum/Ab sample + virus), dividing this result by the average RLU of virus only wells (cell + virus column) and multiplying by 100. Background is subtracted from all test wells using the average RLU from the uninfected control wells (cells only column) before calculating the percent neutralization. Neutralizing serum antibody titers are expressed as the serum dilution/antibody concentration required to achieve 50% neutralization and calculated using a dose-response curve fit with a 5-parameter nonlinear function.

Neutralization Assays Using CF2 Cells

Neutralization assays using CF2 cells were performed as described previously (Crooks et al., 2015). On the day prior to the assay, 96 well plates were seeded with 200 μL of CF2Th.CD4.CCR5 cells at $1x10^5$/ml per well. On the day of the assay, virus was incubated with serially diluted mAbs or serum for 1 hr at 37°C. The virus:antibody/serum mixture was then added to plates seeded with CF2 cells, spinoculated at 300Xg for 15 min, and incubated for 3 days at 37°C. Luciferase activity was measured using the Promega Luciferase Assay System reagent.

HEp-2 Cell Staining

Autoreactivity staining assays were performed on HEp-2 cells per the manufacturer recommendations (Zeus Scientific). MAbs were diluted to 50 and 25 μg/ml using SAVe Diluent. 20 μL of the appropriate dilution was coated onto cells fixed on the slide and incubated for 30 min at room temperature in a humidified chamber. Slides were rinsed in 1X PBS, washed twice in 1X PBS in Coplin jars for 3-5 min and then stained with 20 μL of FITC-conjugated secondary antibody for 30 min in a humidified chamber. Slides were rinsed in 1X PBS, washed twice in 1X PBS in Coplin jars for 3-5 min and mounted with 15 μL of mounting media per well and a cover glass (Thermo Scientific). Slides were imaged on a Nikon Eclipse E800 microscope at 20X in the RGB mode for 2 s using SPOT 5.0 software (SPOT Imaging). VRC01, 4E10, VRC07-523 and VRC07-G54W were used as control mAbs for staining and given a score of 0, 1, 2 and 3 respectively based on their staining intensity. Test antibodies were assigned scores based on visual comparisons of staining intensity to the control antibodies.

Cardiolipin ELISA

mAb binding to cardiolipin was tested by ELISA per the manufacturer's protocol (Inova Diagnostics). Starting at 100 μg/ml, mAbs were tested in a 3-fold series. Assays were validated using positive and negative controls and standards provided in the kit. OD values were converted to IgG anti-phospholipid (GPL) units by linear regression. 4E10 and VRC01 were used as additional positive and negative controls. Cardiolipin binding was scored as follows: no binding for < 15 GPL, indeterminate for 15-20 GPL, low positive for 20-80 GPL and high positive for > 80 GPL.

Genetic Clustering and Phylogenetic Analysis

mAb sequences were aligned by ClustalOmega, followed by ClustalW-Phylogeny and Dendroscope (Huson et al., 2007) to generate and display the phylogenetic tree. mAb lineages were inferred using *Cloanalyst* (http://www.bu.edu/computationalimmunology). Briefly, DNA Maximum Likelihood (DNAML) from the Phylip molecular evolution suite was used to find the maximum likelihood tree using the γ and κ chains together, with mutation rates differing by chain and varying by site. The inferred ancestor (IA) and intermediates were determined by computing the Bayesian posterior probability over all possible sequences representing unmutated immunoglobulin variable-region gene rearrangements.

Blue Native PAGE-Western Blot

VLPs were solubilized in 0.12% Triton X-100 in 1 mM EDTA/1.5 M aminocaproic acid with a protease inhibitor cocktail (P-2714; Sigma). An equal volume of 2X sample buffer (100 mM morpholinepropanesulfonic acid, 100 mM Tris-HCl, pH 7.7, 40% glycerol, and 0.1% Coomassie blue) was added. Samples were then loaded onto a 4%–12% Bis-Tris NuPAGE gel (Thermo Fisher) and separated at 4°C for 3 hr at 100V. The gel was then blotted onto polyvinylidene difluoride and destained with a solution containing 35% methanol and 10% acetic acid followed by 100% methanol until blue stain was removed. The blot was blocked using 4% nonfat milk in PBS for 1 hr at room temperature and probed with mAbs 2G12, b12, 39F, 2F5 and 4E10 at 1μg/ml each. The blot was developed with anti-human Fc alkaline phosphatase conjugate (Jackson ImmunoResearch) diluted 1:5,000 in 2% milk in TBS-T followed by SigmaFast BCIP/NBT substrate (Sigma).

In BN-PAGE "shift" assays (Moore et al., 2006; Tong et al., 2012) mAbs were incubated at 37°C for 1 hr with 12.5 μg gp120 equivalents of Env that was liberated from VLPs by adding 1% Triton X-100. Complexes were then resolved by BN-PAGE-Western blot as above and probed with a cocktail of biotinylated mAbs (b12, 2G12 and 4E10) followed by a streptavidin-alkaline phosphatase conjugate and BCIP/NBT.

Negative-stain EM

VRC38 IgG or monovalent Fab was incubated overnight in Tris-buffered saline (TBS) containing 50mM Tris, 150mM NaCl, pH 7.4) at room temperature with BG505 or B41 SOSIP.664 gp140 trimers (Pugach et al., 2015) at a 10X molar excess of mAb. Samples were then diluted to ~0.01mg/ml in TBS and applied to a plasma-cleaned carbon-coated Cu400 mesh grid (Electron Microscopy Sciences) for about 10 s. Nano-W stain (NanoProbes) was applied for 7 s, blotted with filter paper, and a fresh drop applied for

an additional 15 s before blotting. Image collection and data processing was performed as described elsewhere (de Taeye et al., 2015) on either an FEI Tecnai T12 microscope (2.05 Å/pixel; 52,000X magnification) or FEI Talos microscope (1.57Å/pixel; 92,000X magnification). 2D class averages for these datasets and other data (Doria-Rose et al., 2014; Julien et al., 2013; Sok et al., 2014) were generated by Iterative MSA/MRA (Ogura et al., 2003) or SPARX ISAC methods (Yang et al., 2012). Figures were created using UCSF Chimera (Pettersen et al., 2004).

Structural Analysis

To form VRC38-1FD6-WITO-V1V2 complexes, 3mg of purified VRC38.01 HRV3C mutant IgG was bound to 750 mL Protein A Plus Agarose (Pierce) in a disposable 10ml column. 10mg of V1V2 scaffold, produced in GnTI- cells, was then added. Misfolded or improperly glycosylated scaffold remained unbound to Ab and was flushed with 5 column volumes of PBS. The column was capped and 20 μL of HRV3C protease at 2U/μl was added in 1ml of PBS. After 2 hr at room temperature, the resin was drained, the eluate collected and passed over a 16/60 S200 column in buffer containing 5mM HEPES 7.5, 50mM NaCl, and 0.02% NaN_3. VRC38.01–1FD6-WITO-V1V2 complex fractions were pooled and concentrated to 10mg/ml.

Samples of monovalent VRC38.01 Fab, both unliganded and in complex with 1FD6-WITO-V1V2, were screened for crystallization using 572 conditions from Hampton, Wizard and Precipitant Synergy screens using a Cartesian Honeybee and a mosquito crystallization robot with 0.1 μL of reservoir solution and 0.1 μL of protein solution per condition. Crystals for VRC38.01 Fab obtained in 14% PEG400, 13% PEG8000, 0.1M Tris pH 8.5, 0.1M $MgCl_2$ were flash-frozen in liquid nitrogen with no cryoprotectant. Crystals of VRC38.01–1FD6-WITO-V1V2 obtained in 27% isopropanol, 0.1M imidazole pH 6.5 and 10% PEG8000 were flash-frozen in liquid nitrogen in mother liquor supplemented with 20% 2-methyl-2,4-pentanedial (MPD). Data were collected at 1.00Å using the SER-CAT beamline ID-22 of the Advanced Photon Source, Argonne National Laboratory.

Diffraction data were processed with the HKL2000 suite 6 (HKL Research). A molecular replacement solution for unliganded VRC38.01 obtained with Phenix (www.phenix-online.org) contained one Fab molecule per asymmetric unit in space group $P2_122_1$. The structure of the complex contained one Fab bound to a 1FD6–WITO-V1V2 monomer in space group $P3_221$. Model building was carried out using COOT software (https://www2.mrc-lmb.cam.ac.uk/personal/pemsley/coot/), and was refined with Phenix. Final data collection and refinement statistics are shown in Table S1. The Ramachandran plot determined by Molprobity (http://molprobity.biochem.duke.edu) shows 98.4% of all residues in favored regions and 100% of all residues in allowed regions for the unliganded Fab structure and 96.5% of all residues in favored regions and 99.6% of all residues in allowed regions for the complex structure.

Biolayer Interferometry

BG505.T332N.His8x SOSIP.664 was coated onto a His1K Octet biosensor surface (ForteBio) at 10 μg/ml for 60 s, followed by a baseline for 60 s and an association step with saturating concentrations of various mAbs (50 μg/ml of IgG for 30 min or 50 μg/ml Fab fragments for 45 min). Response values from the last 30 s of the association step were averaged to obtain the saturation binding. Mean binding response and standard deviations from 3 independent experiments were plotted against the known number of binding sites occupied by each mAb or mAb cocktail by regression analysis to generate a standard curve for trimer occupancy.

Surface Plasmon Resonance Analysis

Affinities and kinetics of binding of VRC38.01 Fab and IgG to BG505 DS-SOSIP.664 soluble trimer were assessed by surface plasmon resonance on a Biacore S-200 (GE Healthcare) at 25°C with buffer HBS-EP+ (10mM HEPES, pH 7.4, 150mM NaCl, 3mM EDTA, and 0.05% surfactant P-20). Ab was first immobilized onto two flow cells on a CM5 chip at ~800 response units (RU) with standard amine coupling protocol (GE Healthcare). PGT145 IgG was immobilized as a control to ensure trimer fidelity with BSA immobilized in the reference channel. Trimer, at two-fold dilutions starting from 40nM were injected at a flow rate of 50 μl/min for 4 min and allowed to dissociate for 6 min. The cells were regenerated with 100 μL injections of 3.0M $MgCl_2$ at a flow rate of 50 μl/min. Sensorgrams of the concentration series were corrected with corresponding blank curves and fitted globally with Biacore S200 evaluation software (GE Healthcare) using a 1:1 Langmuir model of binding to highlight the apparent change in affinity from Fab to IgG.

Isothermal Titration Calorimetry

Isothermal titration calorimetry (ITC) was performed using the ITC200 microcalorimeter system (MicroCal). Proteins were dialyzed against filtered PBS before use. The concentration of BG505 native, flexibly linked (NFL) trimer (Sharma et al., 2015) in the sample cell was approximately 25 μM, and that of VRC38.01 Fab in the syringe was approximately 5 μM. Reactions were carried out at 37°C, as previously described (Wu et al., 2010). Briefly, BG505 NFL trimer was titrated to saturation by stepwise addition of 2 μL ligand in the syringe at 120 s intervals at 37°C. The heat evolved upon each injection was obtained from the integral of the calorimetric signal. The values of enthalpy (ΔH) and entropy (ΔS) were obtained by fitting the data to a nonlinear least-squares analysis with Microcal ORIGIN software using a single-site binding model.

Neutralization Fingerprinting Analysis

Published neutralization data for a set of ~200 donor plasma samples (Hraber et al., 2014) was analyzed by using a next-generation neutralization fingerprinting algorithm (Doria-Rose et al., 2017). For a given sample, the approach compares a polyclonal neutralization pattern of a set of diverse viral strains to the neutralization patterns (or fingerprints) of a reference set of broadly neutralizing mAb

specificities, to obtain an estimate of the contribution of each of the reference specificities to polyclonal neutralization (Doria-Rose et al., 2017; Georgiev et al., 2013). Reference broadly neutralizing antibodies were used as previously described (Pancera et al., 2014), with the VRC38 fingerprint as a separate category. We applied computational quality control metrics for filtering out plasma samples for which the predictions were deemed unlikely to be accurate. Specifically, these included metrics for: (i) predicting the presence of dominant novel specificities and (ii) computing a confidence score associated with the computational predictions for each given sample (Doria-Rose et al., 2017). Through this process, the initial set of samples was reduced to 80 samples, which were used for the analysis of Ab specificity frequency. Samples were predicted to have between 1 and 3 specificities from the reference set, and the overall frequency of observing the different reference specificities or pairs of reference specificities were analyzed.

QUANTIFICATION AND STATISTICAL ANALYSIS

For all mAb/serum pseudovirus neutralization assays (Figures 1E, 6D, 6E, S2A, S3B, S4A, S5B, S5F, S6A, S7E, and S7F, and Tables S1, S3, and S5), data were fitted to a 5-parameter asymmetric nonlinear regression model to obtain the IC_{50}, or concentration of mAb/dilution of serum needed to obtain 50% neutralization against a given pseudovirus. For neutralization assays in which a fold-change in IC_{50} imparted by a particular virus mutant, virus treatment, or binding stoichiometry (e.g., IgG versus Fab) was reported (Figures 6D and 6E, S4A, S5B, S5F, and S7E, and Tables S3 and S5), the IC_{50} obtained for one virus/assay condition was divided by the IC_{50} obtained for the other virus/assay condition, as indicated in the figure legends and *y*-axes of data graphs. All neutralization assays were repeated at least 2 times, and data shown are from representative experiments.

Multiple binding assays were performed to investigate VRC38.01 binding to HIV-1 Env trimers and monomers. All ELISAs (Figures 2A–2C, S2C, S2D, S2F, and S3A) were repeated at least two times, and curves shown are from representative experiments. BLI measurements (Figure S4D) were taken over 3 independent experiments, and the means and standard deviations of binding values were plotted. Binding stoichiometry of VRC38.01 IgG and Fab were interpolated from a standard linear regression equation (indicated in the plots) derived from the BLI response data (nm) plotted against number of known IgG/Fab binding sites per trimer. Association and dissociation kinetics derived from SPR data (Figure S4B) were fitted to a 1:1 Langmuir model using Biacore S200 software, and data from a representative of 3 independent experiments is shown. For ITC, enthalpy and entropy values were interpolated from a nonlinear least-squares analysis using Microcal ORIGIN software using a single-site binding model, and results shown are a representative of 3 independent experiments.

DATA AND SOFTWARE AVAILABILITY

The accession numbers for the VRC38.01-VRC38.14 heavy chain sequences reported in this paper are Genbank: KY_905214, Genbank: KY_905215, Genbank: KY_905216, Genbank: KY_905217, Genbank: KY_905218, Genbank: KY_905219, Genbank: KY_905220, Genbank: KY_905221, Genbank: KY_905222, Genbank: KY_905223, Genbank: KY_905224, Genbank: KY_905225, Genbank: KY_905226, and Genbank: KY_905227. Accession numbers for the VRC38.01-VRC38.11 light chain sequences are Genbank: KY_905228, Genbank: KY_905229, Genbank: KY_905230, Genbank: KY_905231, Genbank: KY_905232, Genbank: KY_905233, Genbank: KY_905234, Genbank: KY_905235, Genbank: KY_905236, Genbank: KY_905237, and Genbank: KY_905238. The crystal structures for unliganded N90-VRC38.01 Fab and V1V2-scaffold complex have been deposited in Protein Data Bank with ID codes PDB: 5EWI and PDB: 5VGJ, respectively. Sequences for antibodies were confirmed as being received on April 7th, 2017. The crystal structures are expected to be accessible in ~2 weeks from now.